Magnetic Field Optimization From Limited Data

Matthieu Chassot

Master of Science
Artificial Intelligence
School of Informatics
University of Edinburgh
2009

ABSTRACT

When a sensor coil is placed in the field of an electromagnetic transmitter, a voltage is induced and may be measured. The amplitude of this voltage depends on the distance from the transmitter and the angle between the axes of the transmitter and the sensor. This relationship between the state of the coil and the voltages, known as the dipole model, can be exploited to track sensor coils in the space. ElectroMagnetic Articulography (EMA) uses this principle. It consists in measuring and representing graphically the mechanics of speech using sensor coils moved through the magnetic field induced by electromagnetic transmitters. The Carstens AG-500 EMA machine aims to provide 3-dimensional tracking of coils with 5 degrees of freedom and is used in speech mechanics research. The tracking process relies on optimization algorithms run to minimize the error between the measured voltages and the predicted ones using the dipole model. However, there is evidence to suggest that the dipole model may not match the actual magnetic field and then induces inaccurate tracking.

In this project, the feasibility of building a ***trainable*** model of the magnetic field is investigated. Using data sets sampled from the dipole model, different neural networks were trained and their performances compared. The objective of having such a model of the magnetic field would be to allow further optimization given some new data. A solution based on a constrained tracking of several sensor coils and an Unscented Kalman filtering algorithm is presented. Several coils were fixed relative to each other on a rigid body and moved through the measurement field of the AG-500. Using the knowledge of the fixed arrangement of the sensors on the block, the movement of this rigid body could be tracked. Finally, several methods to discover the arrangements of coils fixed on a rigid device were tested.

The three solutions described above are part of a potential new calibration procedure aimed at accommodating any magnetic field distortions created by perturbations from the environment.

ACKNOWLEDGEMENTS

I would like to thank my supervisor Korin Richmond, for his precious suggestions, constant support and encouragement that led me to this stage of the project; Joanna Tomasik for her valuable help that allowed me to come here to study and for having been an exceptional tutor; and finally my parents, for believing in me and constantly supporting me.

DECLARATION

I declare that this thesis was composed by myself, that the work contained herein is my own except where explicitly stated otherwise in the text, and that this work has not been submitted for any other degree or professional qualification except as specified.

Matthieu Chassot

Table of Contents

Chapter 1 Introduction 1

1.1 Electromagnetic Articulography 1

1.2 The AG500 Electro-Magnetic Articulography system 3

1.2.1 The dipole model 4

1.2.2 Calibration 5

1.3 The objectives 6

Chapter 2 Background 8

2.1.1 An inaccurate field model 8

2.1.2 Correcting the magnetic field model 8

2.1.3 Building the magnetic field model from data 9

2.2 Artificial Neural Networks 10

2.2.1 Analysis of several neural networks: Scattered Data Interpolation 11

Chapter 3 Training Neural Networks to use with the AG-500 13

3.1 Creating the data sets 13

3.2 Methods to train the networks 15

3.3 Selection of Neural Networks 17

3.3.1 Function Complexity 18

3.3.2 Training the *VoltNets* 21

3.3.3 Training the *FieldNets* 22

Chapter 4 Accuracy Assessment 24

4.1 Tracking the coils in the magnetic field 24

4.2 Unscented Kalman Filtering 24

4.2.1 Kalman Filtering 25

4.2.2 Unscented Transform 27

4.3 Unconstrained Tracking 30

4.4 Accuracy of the new field models 32

4.4.1 Networks interpolating the voltages 38
4.4.2 Networks interpolating the magnetic field 42
Chapter 5 Optimizing the field model 46
5.1 A constrained tracking problem 46
5.1.1 Tracking the woodblock in the field 48
5.1.2 Several alternatives to track the woodblock 50
5.2 An EM approach to optimize the tracking of the woodblock 55
5.2.1 Measuring the positions and orientations of the coils on the woodblock 56
Chapter 6 Conclusion 64
6.1 Summary of the project 64
6.2 Results 65
6.2.1 Interpolated observation model 65
6.2.2 Creating a new training data set from measured data 66
6.3 Further Works 68
Appendix 70
Reverse Hardy's Multi-Quadrics 70
Dual Hidden-Layered MLP 70
References 72

List of figures

Figure 1 - The AG-500 device 3
Figure 2 - AG-500 Coordinate System & Positions of the transmitters 4
Figure 3 - Magnetic Latitude 5
Figure 4 - Artificial Neural Network Diagram 11
Figure 5 - Spherical Coordinate System 13
Figure 6 - Log of the training Error with the angles fixed to 0° 19
Figure 7 - Log of the training Error with theta varying and phi fixed to 0° 20
Figure 8 - Log of the training Error with 5 degrees of freedom 20
Figure 9 - Arrangement of the coils on the woodblock 32
Figure 10 - Distance between coils 3 & 4 tracked with the calcamps function 33
Figure 11 - 3D Plot of the movements of the 4 coils 35
Figure 12 - RMS error of the coil 1 36
Figure 13 - RMS error of the coil 2 36
Figure 14 - RMS error of the coil 3 37
Figure 15 - RMS error of the coil 4 37
Figure 16 - Distance between coils 3 & 4 – VoltNets 42
Figure 17 - Distance between coils 3 & 4 - FieldNets 44
Figure 18 - Euler Angles 47
Figure 19 - Woodblock with 4 coils and the local coordinate system 49
Figure 20 - Local positions on X-axis - Block tracked with 3 coils 52
Figure 21 - Local positions on Y-axis - Block tracked with 3 coils 52
Figure 22 - Local positions on Z-axis - Block tracked with 3 coils 53
Figure 23 - Local positions on X-axis - Block tracked with 4 coils 53
Figure 24 - Local positions on Y-axis - Block tracked with 4 coils 54
Figure 25 - Local positions on Z-axis - Block tracked with 4 coils 54
Figure 26 - Optimization of the distances between the coils 58
Figure 27 - Local positions of the coils while distances are optimized 60
Figure 28 - Jointly optimized local positions 62
Figure 29 - Distance between the coils 1 and 3 tracked with the Joint UKF 63

List of tables

Table 1 - Training Data Set for the VoltNets 14
Table 2 - Training Data Set for the FieldNets 15
Table 3 - Comparison of the complexity of the state-to-voltage function 19
Table 4 - Comparison of different trained VoltNets 22
Table 5 - Comparison of different trained FieldNets 23
Table 6 - Distances between coils using the VoltNets 38
Table 7 - Distances between coils using the FieldNets 43
Table 8 - Intended local positions of the coils on the woodblock 49
Table 9 - Mean of the optimized distances 58

Chapter 1 Introduction

Speech Synthesis has now become quite a common thing in our lives. The reader will probably remember the hologram in the first Star Wars trilogy when the hero receives a message and that the face expression is very accurate. However, at this time, the hologram was just a pre recorded movie with some post processing effects to give the impression that the person is not in the same place. There is still not a device that is capable of reproducing the facial expressions for any spoken sentence. In order to do that, one must know all the movements of the jaw, the tongue and the lips. There are some ways to do that, by using optical devices, but this is not adequate to study articulography movements inside the mouth, which is quite important for all the applications it allows (speech training for deaf people, communication in noisy environments where microphones are unusable,...). Fortunately, other means of recording these movements inside and outside the vocal tract have been developed. They rely on an inductive measuring principle.

1.1 Electromagnetic Articulography

Electromagnetic transmitters driven by alternating current produce an inhomogeneous alternating magnetic field. When a receiving coil sensor is placed in this field, an alternating voltage is induced. Given the distance from the transmitter and the orientation of the sensor relative to the transmitter, we may calculate the amplitude of the voltage that is induced between the two ends of the sensor coil. A simple approach to explain these properties is to use the *dipole* model which describes the magnetic flux density to be inversely proportional to the cube of the distance from the transmitter. The induced voltage also depends on the orientation of the sensor, so that it is proportional to the scalar product between the magnetic field vector and the unit vector that describes the orientation of the sensor.

Therefore, given the position and orientation of the coils relative to those of the transmitter, there is a simple way to calculate accurately the voltages which we expect to be induced. However, this function that provides the amplitude of the voltage given the position and the orientation of the sensor is not linear, and there is no simple way to invert it. Thus, inferring the state of the coil in the magnetic field from measurements of the induced voltage is not direct. In order to find positions and orientations of the sensor coil while the only data

that can be observed are the voltages, one needs to use iterative non-linear optimization algorithms. Those methods aim to find an optimum state that minimizes the error between the measured voltage and the voltage that is predicted at this position and this orientation. The best outcome happens when the error is null, which means that the algorithm has ended up with a state that is an antecedent of the measured voltage (though this does not necessarily mean this is the only solution). In practice, the algorithm may find a locally optimum solution and fail to converge on the globally best solution.

As already mentioned (and described more accurately in section 1.2.1), the relationship between the state of the coil and the voltage is highly non-linear, which increases the difficulty of predicting the state given the voltage. The voltage varies in a one-dimensional space while the coil has 5 degrees of freedom, 3 Cartesian coordinates and 2 angles. Therefore, one transmitter alone does not provide enough information to locate the sensor. Many positions around the transmitter can be associated with the same voltage amplitude. This problem can be solved by using several transmitters set at strategic positions. The *AG-500*, described in section 1.2, uses 6 transmitters, and so to estimate sensors' positions and orientations, we essentially have 6 equations in 5 unknown variables to allow a 3 dimensional localization.

1.2 The AG500 Electro-Magnetic Articulography system

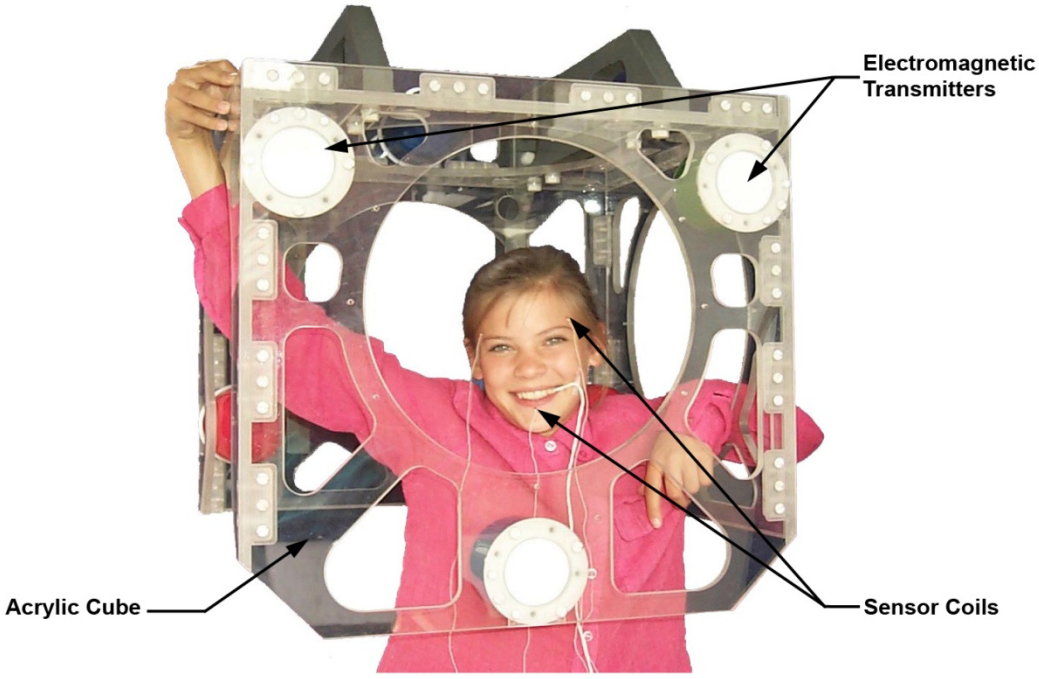

Figure 1 - The AG-500 device
(Photo from (Carstens)*)*

The AG500 (Figure 1) is the most developed 3 dimensional *Electro Magnetic Articulography* (EMA) system, and there is no other technology available that is fully comparable in capabilities with this device. It provides real time motion tracking in 5 degrees of freedom, which are the 3 Cartesian coordinates and 2 orientation angles. The device comprises a cube-shaped acrylic glass structure with six transmitter coils arranged spherically such that the receiver coil axis is never perpendicular to more than one transmitter at a time (there is a right angle between every pair of transmitters) (see Figure 2). Each transmitter has a unique frequency, ranging from 7.5 to 13.75 kHz so that, using frequency demodulation, one can measure the voltage induced in the sensor coil corresponding to each transmitter separately (Zierdt, Kaburagi, Hoole, Honda, & Tillman, 2000).

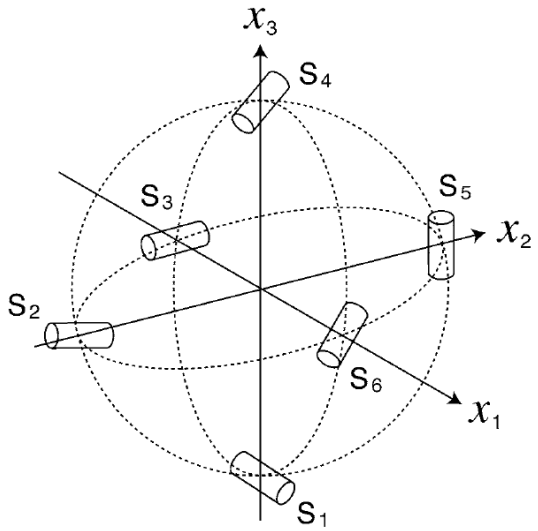

Figure 2 - AG-500 Coordinate System & Positions of the transmitters
(Extracted from (Kaburagi, Wakamiya, & Honda, 2005)*)*

The voltages induced can be measured in up to 12 receiver coils at the same time. The voltage measured at the sensors depends on the distance from the transmitter and the angle between the axis of each transmitter and of each sensor. The general method to describe the variation of the voltages is to use the dipole model which is described in section 1.2.1 below. Given the measured voltages in each sensor, Cartesian and angular coordinates of each of them are determined by solving a set of non-linear mathematical equations. Given the magnetic field model or a state-to-voltage function, the expected amplitudes are computed and compared to the measured ones. Then, the determination of the states of the sensors is achieved with some optimization methods in order to minimize the error between the measured voltages and the expected ones. The commonly used optimization methods are Newton's Method, or Leven-Marquardt's Method.

1.2.1 The dipole model

In the original version of the AG-500 implemented by A. Zierdt (Zierdt, Hoole, & Tillman, Development of a system for three-dimensional fleshpoint measurement of speech movements, 1999), the relation between the state (Cartesian and angle coordinates) of the sensor and the amplitudes of the induced voltages is defined with the dipole model. This model describes the magnetic field induced by and around a magnetic dipole, which is a device with a close circulation of electric current. According to this model, the magnetic field vector is governed by the equation:

$$\vec{B}(\vec{m},\vec{r}) = \frac{\mu_0}{4\pi r^3}[3(\vec{m}.\vec{r})\vec{r} - \vec{m}] + \frac{2\mu_0}{3}\vec{m}\delta^3(\vec{r})$$

where:

- $\vec{B}$ is the magnetic field vector at the position defined by $\vec{r}$,
- μ_0 is the permeability of free space,
- $\vec{m}$ is the dipole moment,
- $\vec{r}$ is the vector from the position of the dipole to the position of the sensor,
- $\delta^3(\vec{r})$ is the three-dimensional delta function ($\delta^3(\vec{r}) = 0$, except at $\vec{r} = (0;0;0)$),

Then, if β is the opening angle between axis of the field vector and that of the sensor, the voltage signal is proportional to:

$$V(r,\lambda,\beta) \propto \frac{cos\ (\beta)}{r^3}\sqrt{1 + 3\ sin^2(\lambda)}$$

where λ is the magnetic latitude measured from the dipole axis (see Figure 3).

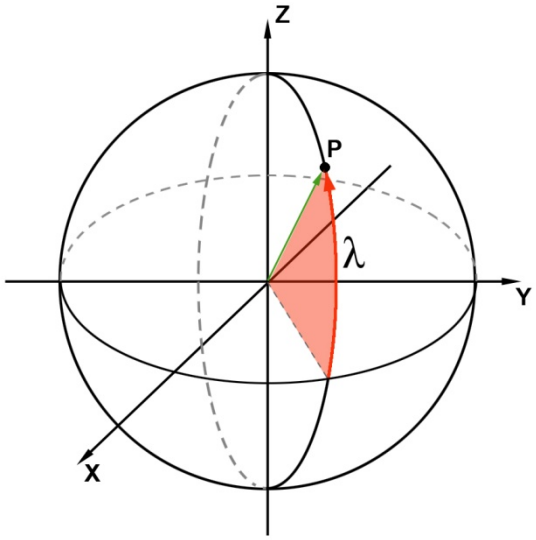

Figure 3 - Magnetic Latitude

1.2.2 Calibration

The system that uses the dipole model requires calibration to define the relationship between the voltage amplitudes and the state of each sensor. The dipole model only defines a relation of proportionality between those two domains and this still remains to be determined. To track the sensors through the magnetic field, the absolute measured signal strength is not important, but in order to run the position calculation algorithm, this amplitude must be calibrated to the expected signals or this would result in an inaccurate

tracking. This calibration factor is usually estimated using a rotating disk with several sensors (see (Carstens) for more details of this procedure).

1.3 The objectives

The AG-500 has been shown to work satisfactorily and is used in research. However, there is room for improvement in the accuracy and the reliability of this device (Yanusova, Green, & Mefferd, 2009). In fact, there are some positional errors that are unacceptable in some localized regions of the measurement field. The dipole model, together with calibration factors found using Autokal (see (Zierdt A. , EMA and the crux of calibration, August 2007)), may not match the true physical properties of the AG-500 system at the time of recording voltages. Those inaccuracies will be illustrated in this project.

As a consequence, one might consider building a representation of the magnetic field based on interpolation methods where voltage measurements are taken at many known positions in the measurement field. Then, interpolation of these is used to give the voltages at any given point. Such representations of the magnetic field can provide satisfactory results as this was presented in (Kaburagi, Wakamiya, & Honda, 2005). However, while this solution proved successful, it has several downsides. Placing 12 coils accurately at many known locations and orientations is an expensive, not convenient and time-consuming method. It is not conceivable that this would be used before every experiment.

A potential solution to the inaccuracies of the dipole model would be to obtain a *trainable* model of the magnetic field that could be further optimized with new data sampled in the measurement field of the AG-500. Ideally, the only data to be used to optimize the trainable model would consist of the *movements of several sensors that are fixed relative to each other* through the measurement space. Unlike the method implemented by T. Kaburagi and al. (Kaburagi, Wakamiya, & Honda, 2005), this solution would be cheap and easy to achieve. Only minimal effort would be required to record the voltages from the movements of the sensor coils *constrained* by being fixed relative to each other. Those measurements would constitute a new training data set. Although we would not know exactly where each sensor coil is in the measurement field, this measured data set would carry the *limited information* that their relative positions and orientations are fixed. Using this knowledge, the trainable model would be further optimized on this data set using machine learning algorithms to match the true magnetic field as closely as possible. In this project, we will use the data from an experiment done with 4 coils. Those 4 coils were fixed on a block with approximately known relative positions and orientations.

However, the critical success factor of the overall method described above is to have confident knowledge about the relative positions and orientations of the coils fixed on a rigid body. While the sensors could be glued with intended dispositions, there might be some degrees of inaccuracy that would make the overall method fail. Therefore, one should refine the knowledge of the relative arrangement. Improving the accuracy of this limited information aimed at optimizing the trainable model would increase the chances of obtaining satisfactory results with the overall method.

Having some solution to derive and refine the coils' arrangements while they are known to be fixed relative to each other would also add another advantage to this overall calibration procedure. When a human subject, who has been glued up with sensor coils, is speaking in the measurement field of the AG-500, coils fixed behind his ears, on his forehead and on the upper part of his jaw stay fixed relative to each other. Unlike a woodblock where it is possible to accurately measure the relative positions and orientations of the sensors, there is no easy and direct way of doing it with the coils glued on somebody's head. Thus, a method that could discover the relative arrangements of those coils would be valuable. In fact, the limited training data used to further optimize the magnetic field model could be directly recorded before any experiment with the AG-500 involving a human subject. The limited knowledge would consist in the movements of coils glued on somebody's head at positions where they stay with the same relative arrangements (behind the ears, on the nose, on the forehead...). These relative dispositions would be discovered from the measured data.

In this project, we tackle the problem of finding a trainable model of the magnetic field. The feasibility of using other models based on regression techniques is tested and their accuracies are compared. The performances will be first evaluated on separate validation data sets, and then using the data from the constrained movement of the 4 coils fixed on a rigid body. These 4 coils stay at the same relative distances from each other during the experiment. Therefore, accurate models must track those coils satisfying these constraints. To be useful, a trainable model of the magnetic field will be expected to perform at least as well as the dipole model currently used with the AG-500.

Then, we focus on the constrained tracking problem of the block where 4 coils were fixed, and investigate the tracking accuracy of the block. This work was based on the assumption that the relative positions and orientation of the 4 coils were known.

Finally, we implement and evaluate some methods to discover the arrangement of the 4 sensors on the rigid body, given that the actual positions and orientations of the coils could slightly differ from the intended ones.

Chapter 2 Background

2.1.1 An inaccurate field model

A good deal of research has been done on how to minimize the error between the measured voltages and the estimated voltages. As this is a non-linear optimization problem, estimating a sensor's position and orientation requires using non-linear methods to invert the function that predicts the voltage given the position and the orientation of the sensor.

The magnetic field is highly sensitive to any perturbation. Any metal in the area modifies the pattern of the field, and its amplitude. Thus, researchers know that there could be some errors modelling the field and that it must be improved. That is why the designers of the AG-500 have implemented a calibration procedure which is advised to be performed before each experiment to reduce error.

This might also suggest that the dipole model is not very adequate for this device. Previous experiments have shown that using it can lead to considerable errors. In (Yanusova, Green, & Mefferd, 2009), Y. Yunusova reports the errors in the estimated trajectories of sensors that are moved through a circular trajectory. Given the measurements of the voltages, these estimated trajectories are not perfect circles as there are supposed to be. There are some explanations to that, apart from the potentially inaccurate dipole model. The magnetic fields created by the six transmitters can interfere, probably because of the mutual induction between the coils, which makes the actual magnetic field deviate from the theoretical one.

2.1.2 Correcting the magnetic field model

In (Zachmann, 1997), G. Zachmann deals with a way of correcting the estimation of the sensor's position to make up for the distortion of the magnetic field. He focused on an algorithm that could compensate for the inaccuracy of the field model in a $(2.4\text{m})^3$-cave. He measured the magnetic field induced in the cave at 144 points placed on a regular lattice. Then, using these sampled data and an algorithm based on global scattered data interpolation, he built a representation of the magnetic field model and obtained method to track sensors with higher accuracy. Nevertheless, tracking the positions of a sensor in such an environment has a different application to articulography. This is used to create Virtual Reality, but this exploits the same underlying principles. G. Zachmann obtained some

improvement on the tracking accuracy, which suggested that the magnetic field model could be improved. Nevertheless, given that the data points were measured in a $(2.4m)^3$-cave, the standards are not the same as for the AG-500 and an error of 2-5cm in tracking the sensor's positions is quite high compared to the average error of the current AG-500.

2.1.3 Building the magnetic field model from data

T. Kaburagi and al. (Kaburagi, Wakamiya, & Honda, 2005) commented on the potential limitations of the dipole model representing the magnetic field of the AG-500. They suggested changing the field model itself and utilized multivariate B-spline functions to interpolate the magnetic field given some sampled data. They measured the induced signal in a receiver sensor coil that was placed at the crossing points of a grid drawn to cover in a cubic region. This signal was sampled along every Cartesian axis at every crossing point. Given those sampled data points, they built a multivariate B-Spline representation of the magnetic field to be used instead of the dipole model. The expected voltages were calculated from the scalar product between the magnetic field vector and the unit vector that expresses the direction of the axis of the receiver coil. They obtained a higher accuracy with this new model than with the dipole model. The reader must be aware that some of the relative error can also be caused by the magnetic field model. In fact, this error is calculated as the difference between the measured receiver signal and the predicted one using the B-spline representation of the magnetic field, and normalized by the received signal at the origin of the coordinate system as the reference. Therefore, an erroneous predicted voltage can increase the average error.

The work of T. Kaburagi and al. suggests investigating the representation of the magnetic field with other models or methods, such as interpolation methods. This also suggests that a new *state-to-voltage* function that predicts the voltages given the Cartesian and angle coordinates of the sensors could improve the accuracy of the tracking procedure given some sampled data. Using representations of the magnetic field that exploits regression techniques and which can be further optimized given some new sampled data might improve the overall position tracking system. The first step of this method would be to approximate either the magnetic field produced by each transmitter, or the voltages induced from each transmitter and to use those approximations to track the coils through the field. In a second step, those functions to approximate either the magnetic field vector or the induced voltages would be optimized in a data-driven way. One would expect to obtain an average error that is at least as low as the average error that is obtained with the currently used representation based on the dipole model.

2.2 Artificial Neural Networks

In modern Mathematics, much work on approximation exists but there is only a small portion of it that is interesting for the problem of improving the tracking accuracy of the coils through the magnetic field. Given the evidence which indicates that the magnetic field model presents a lack of accuracy and can be improved, a good approximation method for this problem is the Artificial Neural Network (ANN). This is a model for regression where the input vector is forward propagated through a succession of transformations. Each transformation is symbolized by a neuron, which is also called a hidden-unit. In an ANN, neurons can be connected to other ones. When two neurons have a directed connection, this means that one of them computes a function that takes the output of the other neuron as an input. Each neuron computes a function of a linear combination of input variables and/or outputs of other neurons:

$$z_i = h\left(\sum_{j=1}^{M} w_j z_j\right)$$

where:

- z_i is the output of the neuron i,
- $z_j,\ j \in \{1, \dots, M\}$ are an input variables or the outputs of other neurons,
- $w_j,\ j \in \{1, \dots, M\}$ are weighting coefficients,
- h is the function computed by the neuron i,
- M is the total number of inputs of the neuron i.

ANNs are represented by graphical networks as in Figure 4. The function h is called the activation function and defines the type of the ANN. In this problem, we have only used feed-forward ANNs, which means that there is no closed directed cycles in the graphical representation of the networks, and which ensures that the outputs are deterministic functions of the inputs. Neurons can be classified in hidden layers. Then, every neuron computes a function of the outputs of the neurons that belong to the hidden layer immediately below, which creates a hierarchy in the hidden layers.

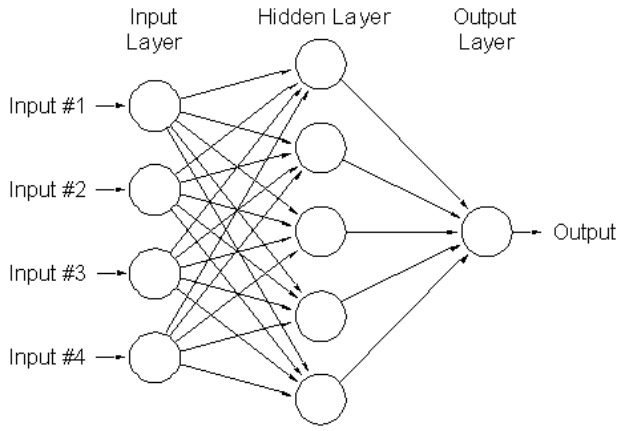

Figure 4 - Artificial Neural Network Diagram
www.odec.ca/projects/2007/stag7m2/images

There has been a huge number of studies regarding feed-forward networks and their potential to approximate arbitrary functions of finite number of real variables. It has be proven (Cybenko, 1989, p. 308) that every bounded continuous function can be approximated with arbitrarily small error by a network with one hidden layer and that any continuous function can be approximated on a compact input domain to arbitrary accuracy by a network with two hidden layers. Neural Networks are therefore said to be *universal approximators*.

2.2.1 Analysis of several neural networks: Scattered Data Interpolation

There exist several sorts of ANNs, and all of them have different properties that make them suitable for one modelling problem or another. The type of the ANN is defined by the basis function that is symbolized by the hidden neurons. Common activation functions for a hidden unit are either sigmoid function (logistic function, arctan...), or Radial-Basis-Functions (RBF) (Gaussian functions, Multi Quadrics function...). The first ones implement one kind of ANNs called Multi-Layered Perceptrons (MLP), and the latter define another type of ANNs which are the RBF networks. The ANNs cited above have been shown to be universal approximators given some conditions (see (Park & Sandberg, Universal Approximation Using Radial-Basis-Function Networks, 1991), (Park & Sandberg, Approximation and Radial-Basis-Function Networks, 1993) and (Cybenko, 1989)).

The Radial Basis function method has been shown to produce high quality solutions in terms of accuracy to the problem of multivariate scattered data interpolation (Lazzaro & Montefusco, 2002). However, this method has been associated with very high computational

cost, as compared to alternative methods such as finite element or multivariate spline interpolation, and also a high computational cost for the training. The Radial Basis Function networks are also highly sensitive to noise.

MLP networks have also been proven to be universal approximators, given enough hidden units and hidden layers. They can also be costly computationally to train and to use if there are several hidden layers.

We also considered another machine learning technique for this problem. Gaussian Processes are usually highly accurate, efficient and easier to train. However, they require storing all the training data points and the values of the kernels on these training data points, which is not appropriate to large scattered data interpolation problems, such as encountered in this study.

Chapter 3 Training Neural Networks to use with the AG-500

3.1 Creating the data sets

In order to train Neural Networks, we required a data set that captures the relationship between the state (position and orientation) of the sensors and some other values that are used to track the sensor in the field. In our case, those values were either the six voltages induced in the coils by each transmitter, or the six magnetic field vectors produced by each transmitter. Knowing that the recommended measurement volume is limited to a sphere with a radius of 150 mm that is centred in the AG-500 cube, we have restricted our data points to this area. Therefore, the data set should describe a reasonably large subset of these positions and orientations of the coils throughout this sphere, which makes a 5-dimensional input space. All data points were created in the following way: a radius ρ and two angles α and β were sampled using a uniform distribution over the intervals [0; 150], [0; 2π] and [0; π] respectively, in order to represent the point in a spherical coordinate system (see Figure 5).

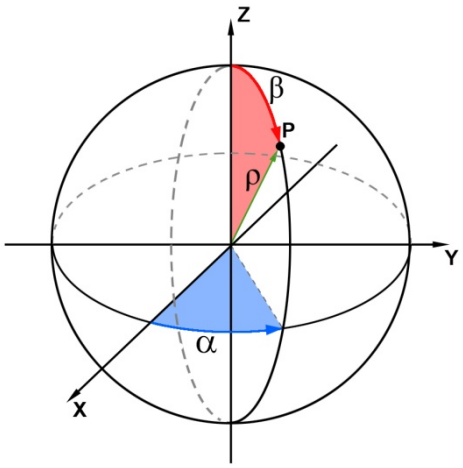

Figure 5 - Spherical Coordinate System

Then, those three parameters were converted to the corresponding Cartesian coordinates. The two angles θ and φ representing the orientation of the coil were also sampled from

uniform distributions over the interval [0; 2π]. Then, depending on the purpose of the neural network, the target values were computed using one of the following methods.

- *Data set to interpolate the voltages*

For the neural networks that map from the state of the coils to the voltages induced by the six transmitters and which we will refer to as the ***VoltNets***, the target values of every input data point were computed using the *calcamps* function of the TAPADM toolbox (Zierdt A. , The 3D-EMA Page). This function takes the state of the coil as input, changes those coordinates to make them correspond to the local coordinate systems of each of the six transmitters. Then it computes the magnetic field vector produced by each of the six transmitters at the position of the coil. The output voltages are proportional to the scalar product between this magnetic field vector and the unit vector that describes the orientation of the coil in the coordinate system of the corresponding transmitter.

$$(V_1, V_2, V_3, V_4, V_5, V_6) = calcamps(x, y, z, \theta, \varphi)$$

- *Data set to interpolate the magnetic field vector*

For the neural networks that maps from the state of the coils to the magnetic field vector and which we will refer to as the ***FieldNets***, a modified version of the *calcamps* function that directly outputs the magnetic field vector corresponding to every transmitter was used.

$$\left(\overrightarrow{\mathcal{M}_1}, \overrightarrow{\mathcal{M}_2}, \overrightarrow{\mathcal{M}_3}, \overrightarrow{\mathcal{M}_4}, \overrightarrow{\mathcal{M}_5}, \overrightarrow{\mathcal{M}_6}\right) = calcfield(x, y, z)$$

Using the two functions described above, a training data set of 100,000 samples and a validation data set of 1,000 samples were created.

In the volume where the points were sampled, the voltages and the magnetic field vector have the following characteristics:

Voltages		V1	V2	V3	V4	V5	V6
Training set	Mean	-0.004	0.001	-0.002	0.007	-0.002	0.005
	Min	-5.17	-7.83	-5.05	-8.46	-5.28	-7.82
	Max	5.12	7.91	5.21	8.19	5.55	8.25
	St. dev	0.764	1.041	0.654	1.123	0.768	0.944

Table 1 - Training Data Set for the VoltNets

Magnetic field		$\|\overrightarrow{H_1}\|$	$\|\overrightarrow{H_2}\|$	$\|\overrightarrow{H_3}\|$	$\|\overrightarrow{H_4}\|$	$\|\overrightarrow{H_5}\|$	$\|\overrightarrow{H_6}\|$
Training set	Mean	30.02	42.96	28.17	44.89	28.42	42.21
	St. dev	17.66	21.81	14.12	25.16	14.29	20.67

Table 2 - Training Data Set for the FieldNets

The target values of these data sets are not noisy; but determined by a function that uses the dipole model. Even though the field model is supposed to be unknown in this problem, creating the data sets in this way ensures that increasing the number of data points will not have a negative effect on the trainings of the neural networks with respect to the accuracy. However, this will add more constraints and will make the training more costly computationally.

In order to evaluate the representation power of different *VoltNets* and *FieldNets*, the data sets were restricted to a line with 1,000 training points, then a plane with 10,000 points. Those intermediate steps revealed that thousands of training cycles were required before the networks gave satisfactory results regarding the error on the validation sets. These pilot experiments also highlighted the need to normalize the input data in order to restrict the range of all inputs from -1 to 1 for the positions, and from 0 to 1 for the angles.

3.2 Methods to train the networks

The two functions which we want to represent using either the *VoltNets* or the *FieldNets* and to compare are two non-linear functions. We had to run optimization algorithms to approximate these functions with the corresponding networks. All computations have been done using Matlab®. The networks and their optimizations have been achieved using the Netlab toolbox (Nabney) which had to be modified to implement other kinds of networks such as Radial-Basis-Function networks with Reverse Hardy's Multiquadrics or dual hidden layers Multi-Layered Perceptrons. All Networks have been optimized using the Scaled Conjugate Gradient algorithm (Møller, 1993) which is already implemented in Netlab. This algorithm is a variation of a conjugate gradient method that uses a Levenberg-Marquardt (Kelley, 1999) approach in order to scale the step size instead of running a line-search algorithm at each step. The scale bounds had been left to their default values set in Netlab ($10^{-15} < \beta < 10^{100}$).

Given the large amount of data points in the training set, running the scaled conjugate gradient algorithm as it has been implemented in Netlab gave rise to memory problems with Matlab®. Therefore, the computation of the weights' gradients using the back-propagation

algorithm had to be slightly modified in order to process the smallest matrices and vectors as possible.

The representation power of a single hidden layer MLP might not be sufficient to this problem. In order to assess these limits, the Netlab toolbox has been enhanced with a set of Matlab® script to utilize dual hidden-layered MLPs (some of the scripts are provided in the appendix). Those scripts are based on the original ones in Netlab and use the Back-Propagation algorithm that is described in (Bishop, 2007, pp. 241-249). While the representation power of dual hidden-layered MLPs is higher than for the single hidden-layered MLPs, the computational cost is also much more significant. The amount of weighting parameters is much more important as there is a weighting parameter for every connection between the neurons of the first hidden layer and the neurons of the second hidden layer. For instance, if the first hidden layer has n neurons and the second hidden layer m neurons, there are (n x m) weighting parameters to represent the relationship between the first and the second hidden layers.

In the original Netlab package, the Radial Basis Function networks can be defined with the one of the following three hidden unit activation functions:

- Gaussian Function: $\phi(r) = exp\left(-\frac{r^2}{2\sigma^2}\right)$
- Thin Plate Spline function: $\phi(r) = r^2 \log(r)$
- Polyharmonic Spline Function of 4th order: $\phi(r) = r^4 \log(r)$

Only the Gaussian functions have shown to be potentially able to interpolate the field vector or the voltages. In fact, the voltages and the amplitude of the magnetic field vector decrease with the distance from the transmitter. Therefore, the thin plate Spine functions and the Polyharmonic Spline Function of 4th order are not adequate for this problem. However, given this remark, we wanted to assess another type of Radial Basis Functions called the Reverse Hardy's Multi-Quadrics (RMQ) functions. Those functions are a close variant of the Hardy's Multi-Quadrics function. According to the comparison of some scattered data interpolation methods in (Franke, 1982), those radial basis functions are one of the most popular scattered data approximation methods. They were also tested in (Gorinevsky & Connolly, 1994) and presented satisfactory results and high accuracy compared to the other scattered data approximation methods. The form of those radial basis functions is as follows:

$$k(\|\vec{r}\|) = \frac{1}{\sqrt{d^2 + \|\vec{r}\|^2}}$$

where d is a scale parameter that has the same role as the standard deviation in a Gaussian radial-basis function, and $\|\vec{r}\|$ represents the norm of the position vector. When those functions are incorporated in a neural network, the output of a hidden neuron which applies this function is the following:

$$k_i(x) = \frac{1}{\sqrt{{d_i}^2 + \|x - c_i\|^2}}$$

where c_i denotes the centre of the radial-basis function k_i of the ith hidden unit, x denotes the input vector that is forward propagated through the neural network. In order to optimize a RBF network with Reverse RMQ functions, the scripts in Netlab had to be adapted. The main modification was done in the *rbfbkp* script, where the components of the gradient of the network with respect to the parameters had to be implemented. The following derivatives were used:

$$\frac{\partial k_i}{\partial c_i}(x) = k_i(x)^3.(x - c_i)$$

$$\frac{\partial k_i}{\partial d_i}(x) = -d_i.k_i(x)^3$$

The details of the scripts can be found in the appendix.

3.3 Selection of Neural Networks

In order to obtain the best accuracy to track the coils in the AG-500, one needs to select the neural networks that ensure the lowest error on a validation set as possible. The training data that were utilized to train the networks are supposed to be non-noisy, given the fact that they were sampled from the magnetic field model itself. Therefore, the error on the training data set should express the accuracy of the neural network with a relatively high fidelity. However, the performances of the different networks were assessed on the validation set which contains 1,000 data points.

The relationship between the state of the coils and the voltages is highly non-linear and the results of our pilot experiments lead us to define a *VoltNet* for every transmitter. Thus, each *VoltNet* takes 5 variables as input and outputs one value. In fact, in the AG-500 measurement field, only the central region is used. The coils are never placed in the corners of the acrylic cube. The relative location of this part of the measurement field is different for every transmitter. It depends on the position and the orientation of the corresponding

transmitter relatively to the AG-500. Therefore, the magnetic field in this central region of the AG-500 is different for every transmitter. This choice of defining one *VoltNet* for every transmitter is justified in section 3.3.1.

Regarding the interpolation of the magnetic field itself, the *FieldNets* were also defined in a similar way as for the voltages. Each *FieldNet* takes 3 variables as inputs which are the 3 Cartesian coordinates, and outputs the 3 Cartesian coordinates that represent the magnetic field vector.

Given those settings, several types of networks were trained on the two data sets described in section 3.1, and their performances were compared.

3.3.1 Function Complexity

The complexity of the function that we want to interpolate given the training data set has been investigated. As this was previously described, the amplitudes of the voltages depend on the position of the sensor relative to the transmitter, but also on the angle between the axis of the coil and the one of the transmitter. Given the model used to represent the positions and the orientations of the coils, there are 5 degrees of freedom: 3 Cartesian coordinates and 2 angles. In order to assess the difficulty to interpolate voltages, the same type of *VoltNet* was trained with different training data sets containing the same number of data points. The first data set contains data points that all have the same orientation, i.e. all the data points have the orientation angles θ and φ set to 0°. The second data set contains the same amount of data points but with θ varying and φ fixed and set to 0°. The third data set still has the same number of data points but both θ and φ vary, as this is described in section 3.1. The results are presented in Table 3. Figure 6 to Figure 8 represent the logarithm of the training error as a function of the training cycles for each of the alternative data sets described above. Each figure plots the logarithm of the training error of every of the 6 networks.

Training Data Set		Cartesian Coordinates with fixed angles	Cartesian Coordinates with one angle varying	Cartesian Coordinates with 2 angles varying
Maximum required Training cycles		1,952	14,197	34,500
Average Training Error (Volt)	V1	1.87E-05	3.53E-04	3.49E-03
	V2	1.87E-05	3.62E-04	6.47E-03
	V3	1.02E-05	3.92E-04	3.58E-03
	V4	8.02E-06	4.09E-04	7.24E-03
	V5	1.53E-05	2.22E-04	2.28E-03
	V6	1.89E-05	5.87E-04	7.53E-03
Average Error on the Validation Set (Volt)	V1	1.63E-05	3.74E-04	4.31E-03
	V2	9.56E-06	4.21E-04	7.15E-03
	V3	7.60E-06	4.76E-04	3.61E-03
	V4	1.62E-05	4.24E-04	7.47E-03
	V5	1.59E-05	2.22E-04	2.46E-03
	V6	1.40E-05	6.19E-04	8.97E-03

Table 3 - Comparison of the complexity of the state-to-voltage function

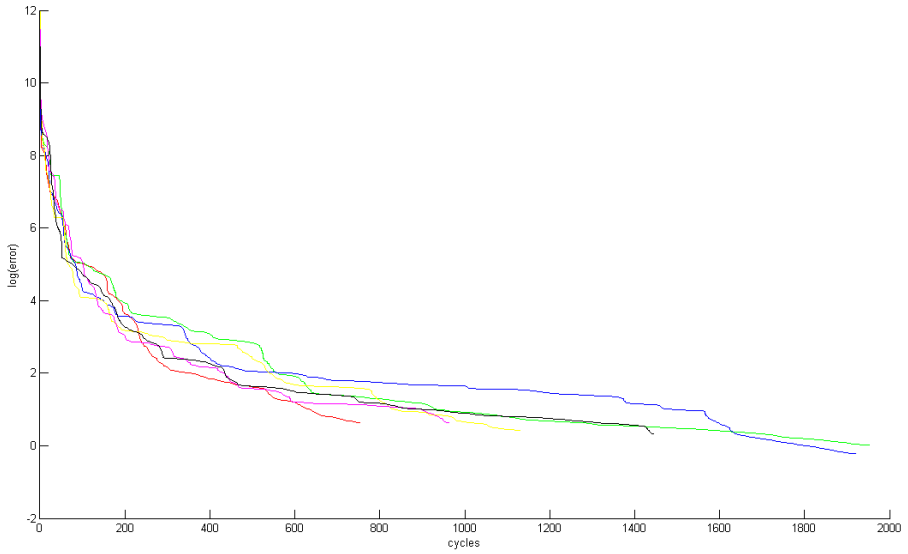

Figure 6 - Log of the training Error with the angles fixed to 0°

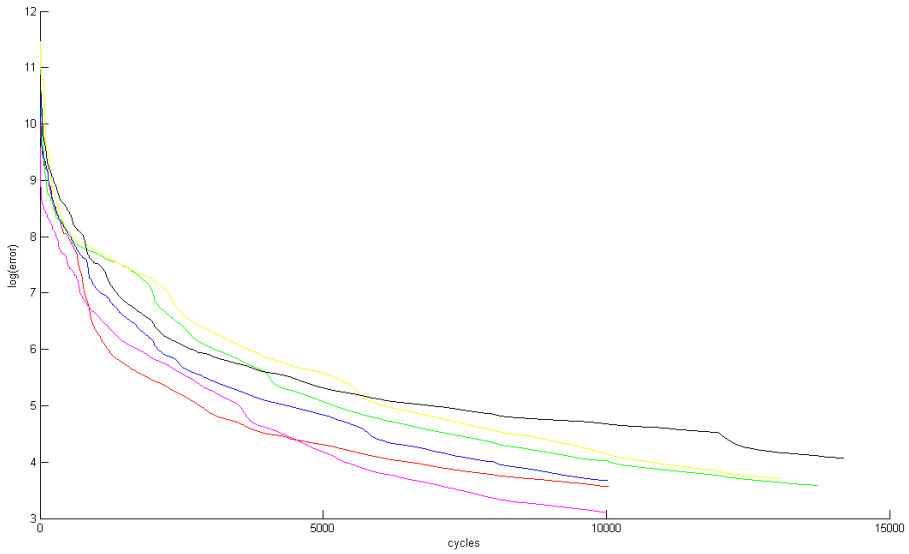

Figure 7 - Log of the training Error with theta varying and phi fixed to 0°

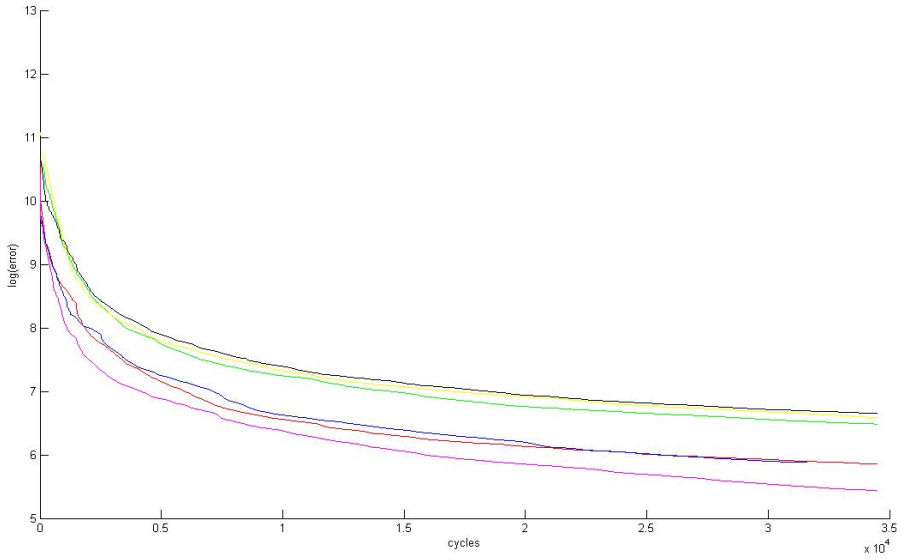

Figure 8 - Log of the training Error with 5 degrees of freedom

The results show that the angles add some significant difficulty in interpolating the function. If the input data had only 3 degrees of freedom, the problem would be much simpler. Furthermore, the cost to train the function would be much more reduced since the space from where to sample is only 3-dimensional instead of 5-dimensional. When one degree of freedom is added, i.e. when one angle varies, the complexity of the state-to-voltage function increases significantly, and training a network with those data is much more costly.

Therefore, this comparison justifies why it has been chosen to train one network for every transmitter.

First, this reduced the complexity of the error function which then depends on one voltage only. Second, this simplified the training process. In fact, the amount of training cycles required to optimize every network with the data set described in section 3.1 was above 10,000. Therefore, this required up to one week to train one type of network on the data set. Every network was trained independently on computers with a capacities equalled to or higher than a Dell OptiPlex 745 Desktop with 2GB of RAM. Those computational requirements were ones of the main problems encountered through this project.

This comparison also suggests that this type of ANNs might be adequate for the *FieldNets*. We will focus on this problem further in this chapter.

3.3.2 Training the *VoltNets*

The first aim of this project was to assess the feasibility of interpolating the voltages with the *VoltNets*. As stated in section 3.3.1, this problem was quite challenging because the 5 degrees of freedom of the input space made the function quite complex. Several types of ANNs have been trained on the data set and their abilities to accurately represent the function were evaluated on the validation data set. More effort has been put on the Multi-Layered perceptrons for this particular function. After the pilot experiments, those ANNs proved to be more adequate to interpolate the voltages. In fact, the radial-basis function networks did not lead to satisfactory results while tested on the validation set. Moreover, as this was presented in section 2.2.1, RBF networks were also highly costly to train, as this can be observed from the maximum number of required training cycles before a local minimum was reached. This can be noted in the results which are presented in Table 4 where the performances on the validation set are compared.

ANN		MLP	MLP DUAL	MLP DUAL	MLP DUAL	MLP DUAL	RBF RMQ	RBF RMQ	RBF Gaussian
Hidden Units		500	200x300	300x200	400x100	50x400	350	500	500
Maximum required Training cycles		19,358	7,537	9,473	7,916	7,043	34,500	21,000	8,000
Average Training Error (Volt)	V1	6.63E-04	1.11E-04	1.44E-04	1.48E-04	1.15E-04	3.49E-03	2.31E-03	1.46E-01
	V2	9.06E-04	1.57E-04	2.15E-04	2.60E-04	1.41E-04	6.47E-03	5.31E-03	3.42E-01
	V3	6.53E-04	1.53E-04	1.87E-04	2.62E-04	2.66E-04	3.58E-03	3.72E-03	1.35E-01
	V4	6.81E-04	1.44E-04	1.78E-04	2.03E-04	1.90E-04	7.24E-03	5.96E-03	3.99E-01
	V5	4.71E-04	2.23E-04	1.43E-04	1.68E-04	1.80E-04	2.28E-03	2.29E-03	9.65E-02
	V6	7.49E-04	1.45E-04	2.03E-04	2.30E-04	1.90E-04	7.53E-03	6.25E-03	3.35E-01
Average Error on the Validation Set (Volt)	V1	8.16E-04	1.20E-04	1.41E-04	1.98E-04	1.23E-04	4.31E-03	2.71E-03	1.63E-01
	V2	8.63E-04	1.98E-04	2.34E-04	2.21E-04	1.47E-04	7.15E-03	5.46E-03	3.06E-01
	V3	6.59E-04	1.49E-04	1.78E-04	2.55E-04	2.86E-04	3.61E-03	3.91E-03	1.35E-01
	V4	5.82E-04	1.47E-04	1.97E-04	2.08E-04	2.39E-04	7.47E-03	7.24E-03	4.27E-01
	V5	3.60E-04	2.49E-04	1.32E-04	1.44E-04	1.89E-04	2.46E-03	2.38E-03	8.86E-02
	V6	9.74E-04	1.52E-04	2.38E-04	2.78E-04	2.19E-04	8.97E-03	7.39E-03	3.29E-01

Table 4 - Comparison of different trained VoltNets

3.3.3 Training the *FieldNets*

As suggested in (Kaburagi, Wakamiya, & Honda, 2005), the dipole model might not match accurately the physical magnetic field in some regions of the space. In order to make up for this inaccuracy, this is possible to interpolate the magnetic field vector in the region of the space were one wants to track the sensors. Therefore, the potential representation of the magnetic field vector by ANNs has been evaluated (see Table 5). While a *VoltNet* with 350 hidden units of Reverse hardy's Multi-Quadrics radial basis function was not adequate, this was not the case for the *FieldNets*. A Gaussian RBF *FieldNet* was also trained on the data set. However, the potential of this network turned out to be limited as one can see in Table 5. The training process was stopped after about 1,000 cycles and without giving as satisfactory results as the other evaluated networks.

ANN		RBF RMQ	RBF Gaussian	MLP DUAL
Hidden Units		350	500	30x30
Maximum required Training cycles		6,811	1,021	9,473
Training Error	V1	4.23E-05	2.29E-02	3.66E-04
	V2	5.48E-05	3.45E-02	6.61E-04
	V3	3.81E-05	1.49E-02	4.56E-04
	V4	4.19E-05	3.76E-02	9.50E-04
	V5	3.57E-05	1.55E-02	4.75E-04
	V6	3.95E-05	2.86E-02	6.12E-04
Error on the Validation Set	M1	3.50E-05	1.26E-02	2.73E-04
	M2	6.57E-05	4.27E-02	1.42E-03
	M3	2.70E-05	1.36E-02	4.90E-04
	M4	4.29E-05	4.47E-02	1.06E-03
	M5	4.29E-05	1.13E-02	5.15E-04
	M6	4.28E-05	2.51E-02	7.05E-04

Table 5 - Comparison of different trained FieldNets

Nevertheless, if we observe the statistics on the training data set (Table 2), we see that the norm of the magnetic field vectors presents a standard deviation in the order of 15. In comparison to the statistics of the voltages (Table 1) for which the standard deviation is close to 1, we see that the scale of the error on the validation set is not the same. Therefore, the *FieldNets* are performing better than the ones interpolating the voltages.

However, the actual performances of all these networks still have to be evaluated with the methods that track the positions and the orientations of the coils. This will be achieved in the next chapter.

Chapter 4 Accuracy Assessment

4.1 Tracking the coils in the magnetic field

To recapitulate, each transmitter induces a signal in each sensor which depends on the position and the axis orientation of the coil relative to the transmitter. For each sensor, six voltages are recorded in order to find the 5 variables that describe the state of the coil. This makes a system of 6 equations with 5 unknown. Those equations are not linear so that the solutions need to be computed numerically using some optimization algorithms. Several methods have been implemented to track the coils in the magnetic fields: the Calcpos program (Carstens software that comes with the AG-500), the TAPADM toolbox and an unscented Kalman Filter approach.

The AG-500 is initially used with the Calcpos program (Carstens). This program uses a standard Newton-method along with a Householder transformation in order to compute the QR decomposition and to estimate the solution of this overdetermined linear equation set.

A. Zierdt developed a Matlab® toolbox called TAPADM ('Three-dimensional Articulographic Position and Align Determination with MATLAB') as an open-source alternative to the Calcpos program (Zierdt A. , The 3D-EMA Page). This toolbox can use other optimization methods than the Newton algorithm, such as the Levenberg-Marquardt algorithm.

K. Richmond (Geng, Richmond, Renals, & Turk, 2009) implemented another approach to track the sensors in the magnetic field. He used an Unscented Kalman filtering algorithm.

4.2 Unscented Kalman Filtering

When the coils are moved through the magnetic field, the voltages are usually recorded with a sampling rate of 200Hz. This makes a discrete-time movement with one sample every 0.005 second. Successive samples are strongly correlated, because they refer to close positions and orientations of the sensor coils. This correlation can be used to track the coils.

4.2.1 Kalman Filtering

The Kalman filter is an efficient recursive filter that estimates the hidden state of a dynamic system from noisy observation measurements. The Kalman Filter operates by propagating the mean and the covariance of the state through time, using the mathematical description of the dynamic system. It is based on a linear discrete-time system given as follows:

State-update Equation: $x_k = F_{k-1}\, x_{k-1} + G_{k-1}\, u_{k-1} + w_{k-1}$

Measurement-update Equation: $y_k = H_k\, x_k + v_k$

where:

- x_k is the hidden state at time *k*,
- y_k is the observation at time *k*,
- F_{k-1} is the state transition model which is applied to the previous hidden state x_{k-1},
- G_{k-1} is the control-input model which is applied to the control vector u_{k-1},
- w_{k-1} is the process noise which is assumed to be drawn from a zero mean multivariate normal distribution with covariance Q_{k-1},
- H_k is the observation model which maps the true hidden state space into the observed space,
- v_k is the observation noise which is assumed to be drawn from a zero mean multivariate normal distribution with covariance R_{k-1},

The noise processes are supposed to be uncorrelated, i.e.:

$$E\left[w_k w_j^T\right] = Q_k \delta_{k-j}$$

$$E\left[v_k v_j^T\right] = R_k \delta_{k-j}$$

$$E\left[v_k w_j^T\right] = 0$$

where δ_{k-j} is the Kronecker delta function, which means that $\delta_{k-j} = 1$ if $k = j$, and $\delta_{k-j} = 0$ if $k \neq j$. The Kalman filter is a recursive estimator as described in the equations above. It uses the state from the previous time and the observation measurement at time k to compute the estimate for the current state. It first estimates an *a priori* hidden state $\hat{x}_k^-$ and an *a posteriori* hidden state $\hat{x}_k^+$ which are the expected value of the state at time k conditioned on all the measurements before (but not including) time k and the expected

value of the state at time k conditioned on all the measurements up to and including time k, respectively.

$$\hat{x}_k^- = E[x_k | y_1, y_2, \dots, y_{k-1}]$$

$$\hat{x}_k^+ = E[x_k | y_1, y_2, \dots, y_k]$$

Given those two estimates, it also computes the covariance matrices of the *a priori* and the *a posterior* estimation errors, noted respectively P_k^- and P_k^+.

$$P_k^- = E[(x_k - \hat{x}_k^-)(x_k - \hat{x}_k^-)^T]$$

$$P_k^+ = E[(x_k - \hat{x}_k^+)(x_k - \hat{x}_k^+)^T]$$

One also needs to define the Kalman Filter gain K_k which adjusts the importance given to the new measurement in the *a posterior* estimation:

$$K_k = P_k^T H_k^T \left(H_k P_k^- H_k^T + R_k\right)^{-1}$$

The initialization of the Kalman filter is achieved as follows:

$$\hat{x}_0^+ = E(x_0)$$

$$P_0^+ = E[(x_0 - \hat{x}_0^+)(x_0 - \hat{x}_0^+)^T]$$

Then, for each time step $k \in \{1,2, \dots, +\infty\}$, the algorithm is run as follows:

$$P_k^- = F_{k-1} P_{k-1}^+ F_{k-1}^T + Q_{k-1}$$

$$K_k = P_k^+ H_k^T R_k^{-1}$$

$$\hat{x}_k^- = F_{k-1} \hat{x}_{k-1}^+ + G_{k-1} u_{k-1}$$

$$\hat{x}_k^+ = \hat{x}_k^- + K_k (y_k - H_k \hat{x}_k^-)$$

$$P_k^+ = (I - K_k H_k) P_k^-$$

The above description of the algorithm is the general one. All the details can be found in (Simon, 2006, pp. 123-148). The main flaw of this algorithm is that it relies on a strong assumption: the state transition equation and the measurement equation are linear. Therefore, this version of the Kalman filter cannot be applied to the problem of tracking the coils in the magnetic field as the relation between the state of the coils (position and orientation) and the measurement equation is non-linear. In order to make up for this linear assumption, one needs to use a modified version of the original Kalman Filter.

4.2.2 Unscented Transform

Most non-trivial real-world systems are non-linear. The non-linearity can stem from the state update equation or the measurement equation or both.

State-update Equation: $x_k = f(x_{k-1}, u_{k-1}) + w_{k-1}$

Measurement-update Equation: $y_k = h(x_k) + v_k$

The non-linear functions f and h cannot be applied to the covariance matrices. In order to make up for these flaws, there exist at least two methods. The Extended Kalman Filter uses matrices of partial derivatives of the functions. But it is difficult to implement and can only be used with systems that are almost linear. For highly non-linear systems, the Unscented Kalman Filter (UKF) has proven to be much more efficient and much more accurate. It uses a deterministic sampling approach in order to propagate mean and covariance information through the non-linear equations. This is known as the unscented transform. The sampled points capture the posterior mean and covariance accurately to the 3rd order according to the Taylor expansion. It was first developed by Simon J. Julier and Jeffrey K. Uhlmann (Julier & Uhlmann, 1997) and further improved by Eric A. Wan and Rudolph Van der Merwe (Wan & Van der Marwe, 2000).

The unscented transformation computes (2L+1) points, where L is the dimension of the variable x that needs to be propagated through a non-linear function. It starts from the assumption that the mean $\bar{x}$ and the covariance matrix P_x are known. Using those, a matrix $\boldsymbol{\chi}$ of (2L+1) sigma vectors χ_i is calculated:

$$\chi_0 = \bar{x}$$

$$\chi_i = \bar{x} + \left(\sqrt{(L+\lambda)P_x}\right)_i, \qquad i = 1, \dots, L$$

$$\chi_i = \bar{x} - \left(\sqrt{(L+\lambda)P_x}\right)_i, \qquad i = L+1, \dots, 2L$$

$$W_0^{(m)} = \frac{\lambda}{L+\lambda}$$

$$W_0^{(c)} = \frac{\lambda}{L+\lambda} + (1 - \alpha^2 + \beta)$$

$$W_i^{(m)} = W_i^{(m)} = \frac{1}{2(L+\lambda)}, \qquad i = 1, \dots, 2L$$

where:

- $\lambda = \alpha^2(L + \kappa) - L$ is a scaling parameter,
- α, β and κ are fixed parameters that are usually set to 10^{-3}, 2 and 0 respectively.
- $\left(\sqrt{(L + \lambda)P_x}\right)_i$ is the i^{th} row of the matrix square root,
- $W_i^{(m)}$ and $W_i^{(c)}$ are weighting parameters used to compute the mean and the covariance respectively.

Those computed sigma points are propagated through the nonlinear function g which can be the state and/or the measurement function:

$$\mathrm{Z}_i = g(\chi_i), \qquad i = 0, \dots, 2L$$

And the mean and the covariance are approximated using the weighting parameters!

$$\bar{\mathrm{Z}} \approx \sum_{i=0}^{2L} W_i^{(m)} \mathrm{Z}_i$$

$$P_{\mathrm{Z}} \approx \sum_{i=0}^{2L} W_i^{(c)} (\mathrm{Z}_i - \bar{\mathrm{Z}})(\mathrm{Z}_i - \bar{\mathrm{Z}})^T$$

This transformation is used along with the Kalman Filter algorithm to form the Unscented Kalman Filter. It first estimates the *a priori* state and the *a priori* measurement given the sigma points computed with the vectors and matrices from the previous time *k-1*. Then, it estimates the observation covariance matrix and the state-observation covariance matrix to calculate the Kalman Gain matrix and achieve the measurement update step. The complete algorithm is described below (see (Haykin, 2001, p. 232)):

Initialization:

$\hat{x}_0$ and P_0 are initialized as with the linear Kalman Filter. Then the process noise and measurement noise are added to the state vector:

$$\hat{x}_0^a = E[x^a] = [\hat{x}_0^T \; 0 \; 0]^T$$

$$P_0^a = E[(x_0^a - \hat{x}_0^a)(x_0^a - \hat{x}_0^a)^T] = \begin{bmatrix} P_0 & 0 & 0 \\ 0 & Q_0 & 0 \\ 0 & 0 & R_0 \end{bmatrix}$$

For each time step $\in \{1, \dots, \infty\}$, the sigma points χ_{k-1}^a of the state augmented with the process and measurement noises are computed as follows:

$$\chi_{k-1}^a = \left[\hat{x}_{k-1}^a \quad \hat{x}_{k-1}^a + \sqrt{(L + \lambda)P_{k-1}^a} \quad \hat{x}_{k-1}^a - \sqrt{(L + \lambda)P_{k-1}^a}\right]$$

For each column $i \in \{1, \dots, 2L+1\}$ of χ_{k-1}^{a} (L is the dimension of the augmented state: $L = dim(x) + dim(v) + dim(w)$):

$$\chi_{k-1_i}^{a} = \begin{bmatrix} \chi_{k-1_i}^{x} \\ \chi_{k-1_i}^{w} \\ \chi_{k-1_i}^{v} \end{bmatrix}$$

Time-update equation:

$$\chi_{k|k-1_i}^{x} = f\left(\chi_{k-1_i}^{x}, u_{k-1}\right) + \chi_{k-1_i}^{w}, \qquad i \in \{1, \dots, 2L+1\}$$

$$\hat{x}_k^- = \sum_{j=0}^{2L} W_j^{(m)} \chi_{k|k-1_{j+1}}^{x}$$

$$P_k^- = \sum_{j=0}^{2L} W_j^{(c)} \left(\chi_{k|k-1_{j+1}}^{x} - \hat{x}_k^-\right)\left(\chi_{k|k-1_{j+1}}^{x} - \hat{x}_k^-\right)^T$$

$$\Upsilon_{k|k-1_i} = h\left(\chi_{k|k-1_i}^{x}\right) + \chi_{k-1_i}^{v}, \qquad i \in \{1, \dots, 2L+1\}$$

$$\hat{y}_k^- = \sum_{j=0}^{2L} W_j^{(m)} \Upsilon_{k|k-1_{j+1}}$$

Measurement-update equations:

$$P_{y_k y_k} = \sum_{j=0}^{2L} W_j^{(c)} \left(\Upsilon_{k|k-1_{j+1}} - \hat{y}_k^-\right)\left(\Upsilon_{k|k-1_{j+1}} - \hat{y}_k^-\right)^T$$

$$P_{x_k y_k} = \sum_{j=0}^{2L} W_j^{(c)} \left(\chi_{k|k-1_{j+1}}^{x} - \hat{x}_k^-\right)\left(\Upsilon_{k|k-1_{j+1}} - \hat{y}_k^-\right)^T$$

$$K_k = P_{x_k y_k} P_{y_k y_k}^{-1}$$

$$\hat{x}_k = \hat{x}_k^- + K_k(y_k - \hat{y}_k^-)$$

$$P_k = P_k^- - K_k P_{y_k y_k} K_k^T$$

This algorithm assumes that the process and the measurement equations are linear with respect to the noise. One will see that this assumption is valid with the problem we are focusing on in this study. The algorithm presented is the general form of the UKF. This can be applied to the problem of tracking the coils in the magnetic field as this is presented in the following section.

4.3 Unconstrained Tracking

The relationship between the state of the sensors and the amplitudes of the voltages that are induced by the transmitters is non-linear. Therefore, in order to apply a Kalman filter to track the coils through the magnetic field, one needs to use the Unscented Kalman filtering algorithm. In fact, the update equation and the measurement equation are as follows:

Update-equation:

$$\begin{bmatrix} x_k \\ y_k \\ z_k \\ \theta_k \\ \varphi_k \end{bmatrix} = I_5 \begin{bmatrix} x_{k-1} \\ y_{k-1} \\ z_{k-1} \\ \theta_{k-1} \\ \varphi_{k-1} \end{bmatrix} + w_{k-1}$$

where $\begin{bmatrix} x_k \\ y_k \\ z_k \\ \theta_k \\ \varphi_k \end{bmatrix}$ are the three Cartesian coordinates and the 2 angle coordinates of the coil at time k, and w_k is the process noise

Measurement equation:

$$\begin{bmatrix} V_{1_k} \\ V_{2_k} \\ V_{3_k} \\ V_{4_k} \\ V_{5_k} \\ V_{6_k} \end{bmatrix} = h\left(\begin{bmatrix} x_k \\ y_k \\ z_k \\ \theta_k \\ \varphi_k \end{bmatrix}\right) + v_k$$

Where:

- V_{i_k} is the i[th] voltage measured on the coil at time k,
- h is the observation model,
- v_k is the observation noise which is assumed to be zero mean Gaussian white noise

The reader can verify that the measurement equation is non-linear and requires using the unscented version of the Kalman filter. In those equations, the state of the coil is set as the hidden state variable, and the six voltages represent the measurements. Given this model and the recorded voltages sampled at 200 Hz, the UKF can be run to track the movement and the orientation of the coil. This model uses a fictitious process noise to represent the movement of the coil. The time-update equation is linear and the state at time k equals the state at time k-1 with addition of some process noise. This allows the filter to place more emphasis on the measurements and ensures that the coil can move according to the measured voltages.

However, it is difficult to estimate the covariance of the process noise that will ensure an accurate tracking process. If a system model has too much noise, this makes it difficult to estimate its state and will end up with a higher tracking error because of the addition of some random movements. But a too little noise will make the system more rigid and prevent it from tracking the true movement of the coil, especially when the sensor is moving rapidly. Therefore, the process noise covariance plays an important role in the tracking process.

Regarding the problem of tracking the coils in the AG-500, the state values approximately vary from -150 mm to +150 mm for the Cartesian coordinates and from 0° to 360° for the angles. The 5 coordinates roughly vary through ranges of the same amplitude. With regard to the problem of tracking each coil independently, a process noise covariance of 0.5 has proven to be adequate, given that the speed of the coils is quite limited and that the sampling rate is high enough. Concerning the measurement-update equation, the noise covariance was set to 10^{-4} and expresses the error in measuring the amplitudes of the voltages.

The three scaling parameters of the UKF, α, β and κ, have been set to fixed values according to the description in (Van der Merwe & Wan, The square-root unscented Kalman Filter for state and parameter-estimation, 2001). α determines the spread of the sigma points around the *a priori* estimation of the state, β is used to incorporate prior knowledge of the distribution of the state x and κ is another scaling parameter. They have been set to the following values:

$$\alpha = 1$$
$$\beta = 2$$
$$\kappa = 0$$

The model described above ignores the exogenous input u_k.

This algorithm was implemented in Matlab® using the existing toolbox ReBEL-0.2.7 which was used under the Academic License (Van der Merwe & Wan, ReBEL, 2006). The initial state covariance was set to $P_0 = 0.75\, I$, and the initial state of the coils was set to the values which were computed with the CalcPos program when the data were acquired. Given those initial conditions and this model, the trajectories of the sensors were computed independently.

4.4 Accuracy of the new field models

The different ANNs trained in sections 3.3.2 and 3.3.3 are aimed at interpolating either the voltages (*VoltNets*), or the magnetic field vector (*FieldNets*). A first evaluation could be done by comparing their performance on a validation set. However, the main purpose of training those ANNs is to use them as a substitute for the dipole model to track the coils in the AG-500 measurement field with at least the same accuracy.

In order to evaluate the performance of the ANNs and to compare them to the *calcamps* function provided with the TAPADM toolbox, we used some data measured with 4 coils that were moved in the AG-500 magnetic field. Those 4 coils were fixed on a woodblock so that their relative positions and orientations remained constant. In particular, the distances between the coils are constant. In this experiment, the block was first held relatively steady in the measurement field. Then, in a second phase, this rigid body was rotated with a backward and forward motion. The rotations had approximately the same amplitudes, but the frequency of the rotations was increased with the time.

A "good" tracking method should calculate a trajectory for each coil that respects the constraint of staying at the same distances from the other coils. The 4 coils were aligned on the block with different orientation, as illustrated in Figure 9.

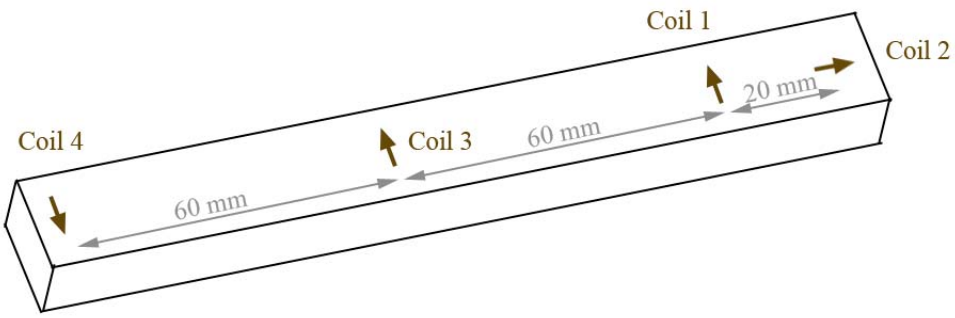

Figure 9 - Arrangement of the coils on the woodblock

Each coil was tracked independently using the UKF algorithm and the corresponding recorded voltages. The UKF algorithm was run with every ANN that we want to assess, and also with the *calcamps* function. Figure 10 shows the distance between the coils 3 and 4 as a function of the time. While the coils are supposed to stay at the same distance, this figures shows that there is some tracking error when the *calcamps* function is used. In fact, the

distance ranges approximately from 56 mm to 63 mm while it should remain fixed to a value close to 60 mm.

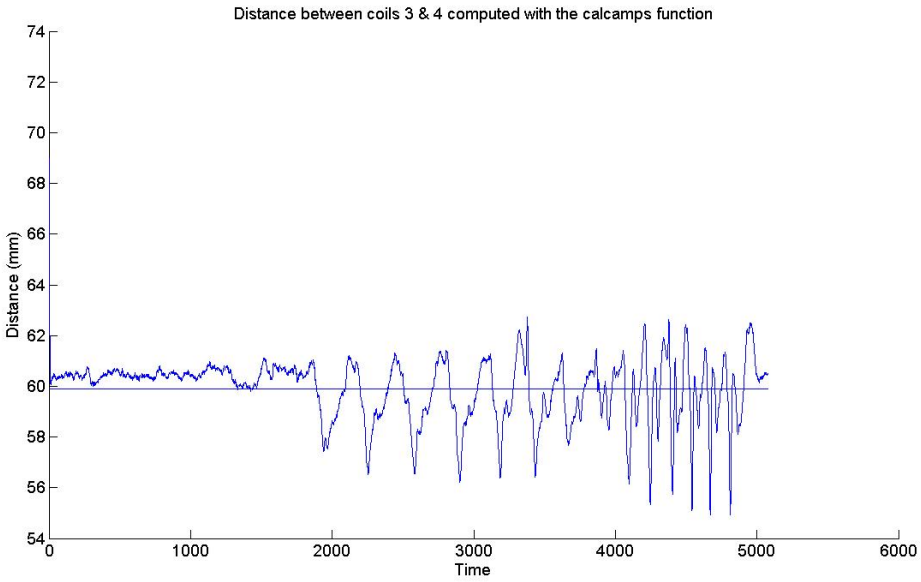

Figure 10 - Distance between coils 3 & 4 tracked with the calcamps function

In the following paragraphs, the performances of the trained *VoltNets* and *FieldNets* are evaluated using the distances between some of the coils on the woodblock. However, as shown in Figure 9, the coil n° 2 was fixed with a different orientation from the other ones. Its trajectory which was computed with the UKF and the observation functions (including the *calcamps* function) presented some irregularities which could be justified with the different orientation and which increased the standard deviation of the distances between this coil and the others.

The 3-dimensional plots in Figure 11 illustrate the inaccurate tracking of this coil. They represent a succession of 6 sampled images from the movement of the 4 coils.

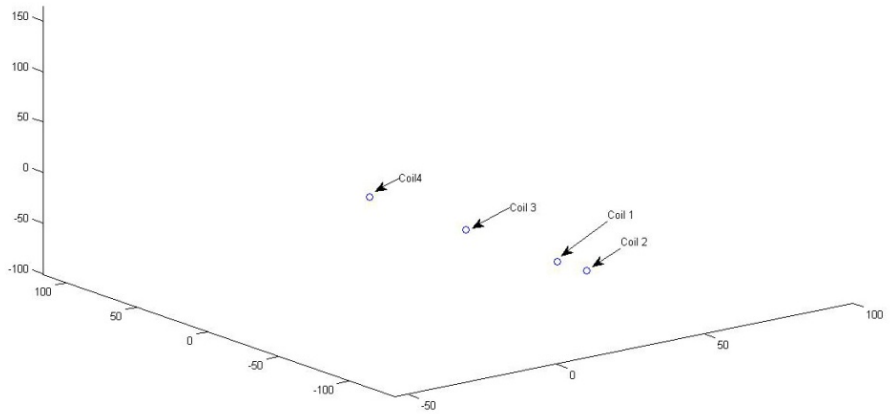

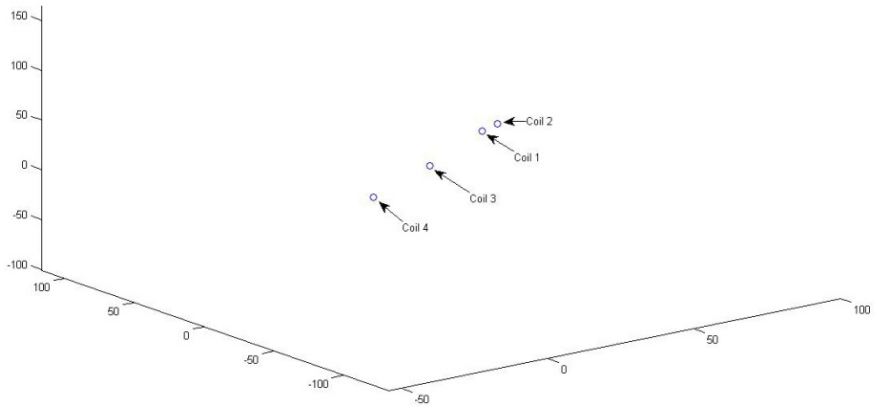
Coil 2
Coil 1
Coil 3
Coil 4

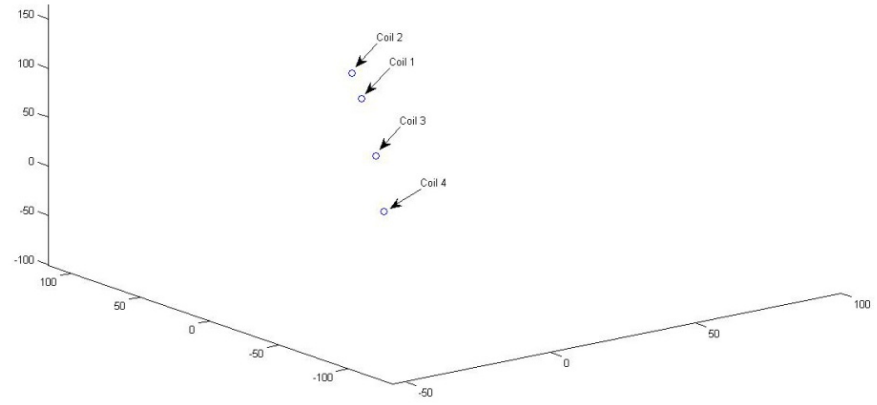
Coil 2
Coil 1
Coil 3
Coil 4

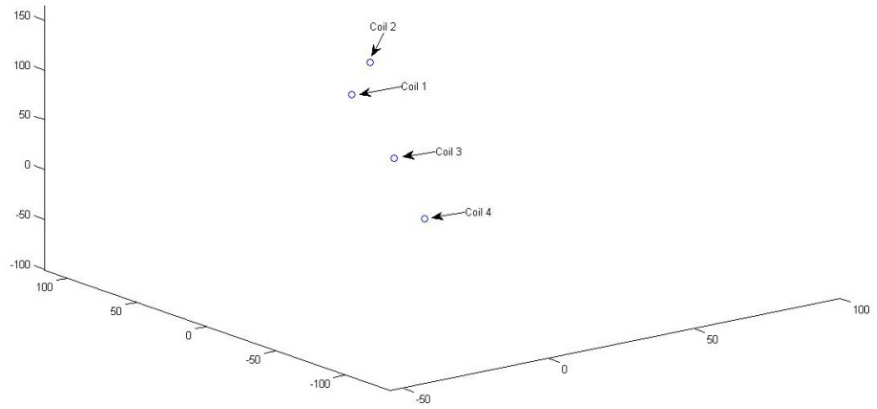
Coil 2
Coil 1
Coil 3
Coil 4

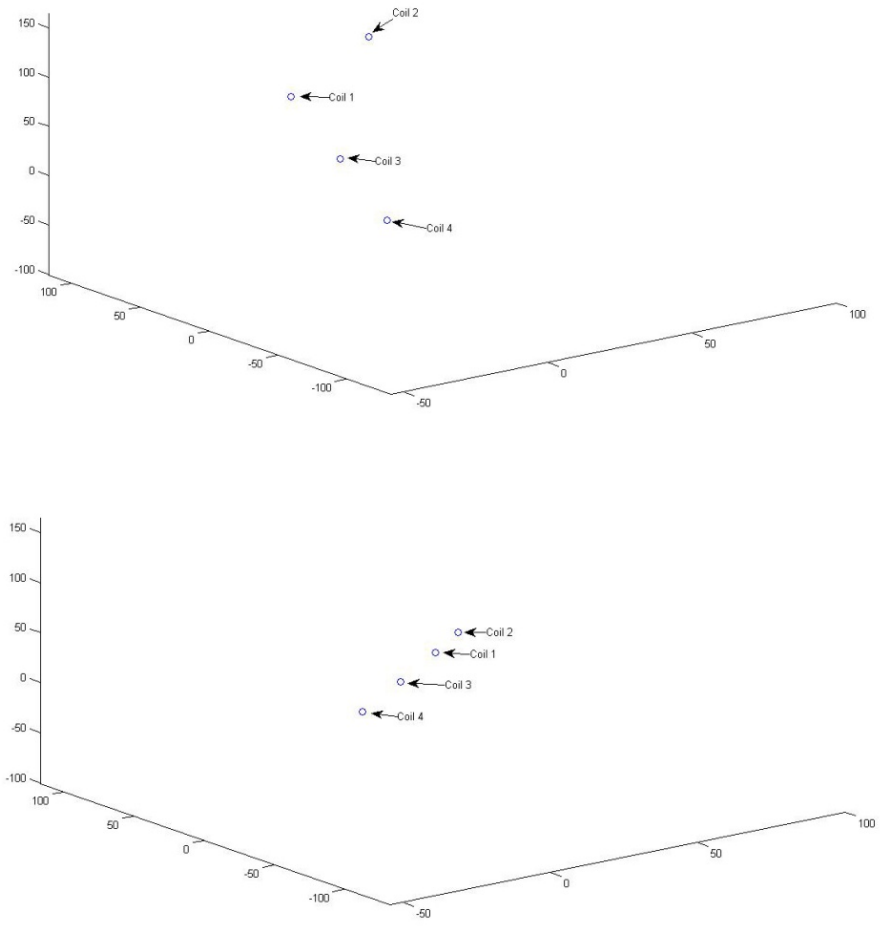

Figure 11 - 3D Plot of the movements of the 4 coils

Figure 11 provides a succession of images sampled from the 3-dimensional movement of the 4 coils tracked independently. In the first 3 images, the block starts rotating towards the vertical position. When the vertical position has been reached, the second coil deviates from the axis where the 3 others are aligned (images 4 and 5). Then, when the block rotates backwards to the horizontal position, the coil n° 2 goes back to an aligned relative position (image 6).

In order to show the inaccuracy of the field model, we focused on the root mean square error between the measured voltages and the predicted ones using the *calcamps* function (based on the dipole model). The RMS error as a function of the time is plotted for each of the coils from Figure 12 to Figure 15.

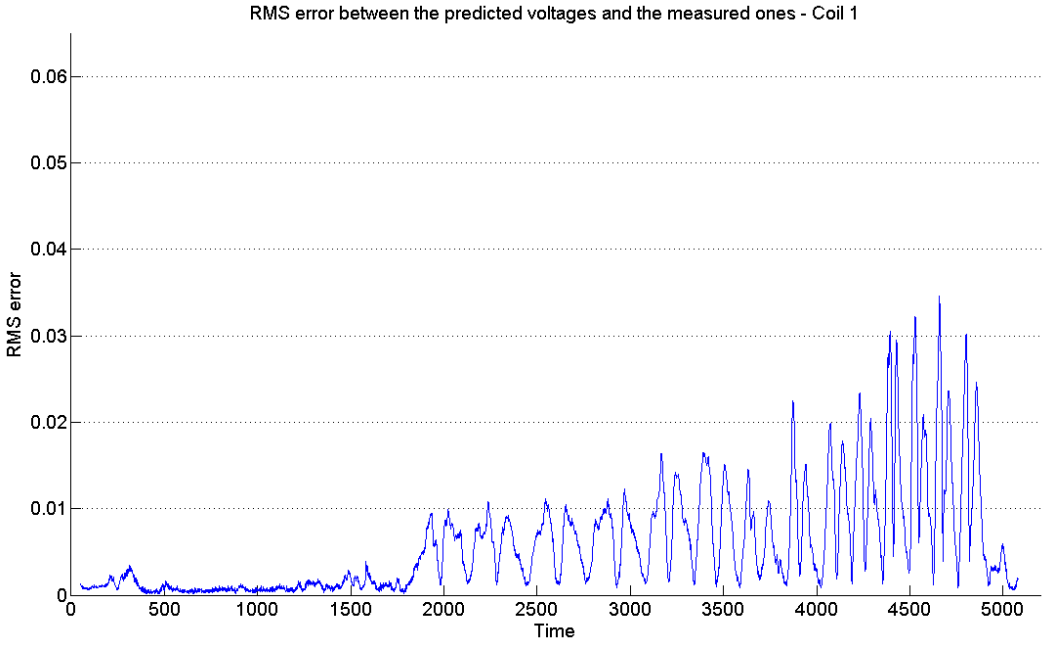

Figure 12 - RMS error of the coil 1

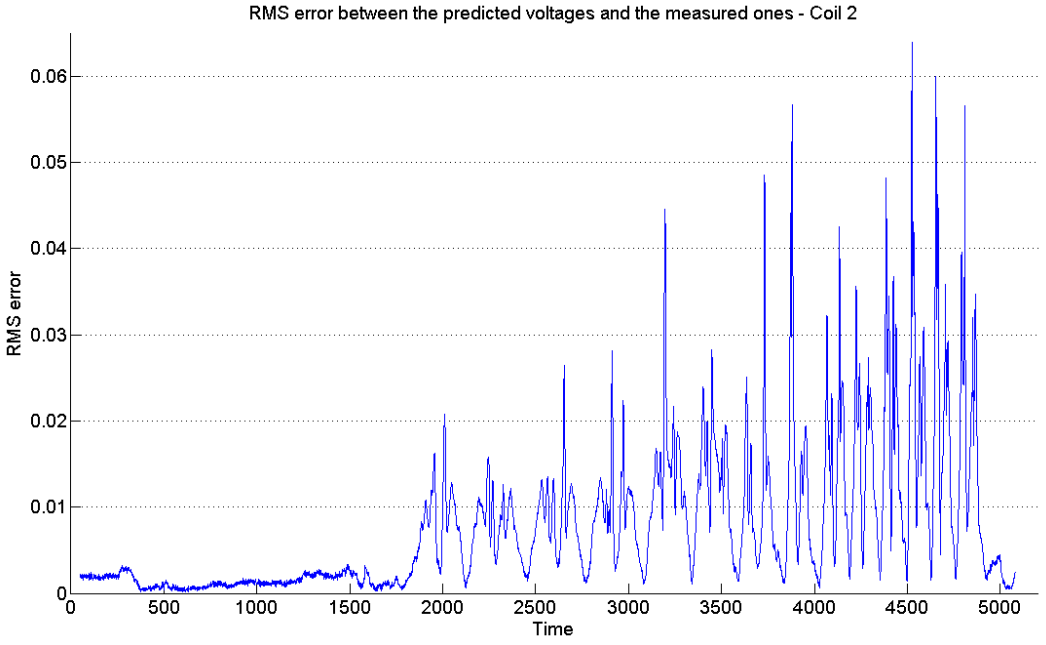

Figure 13 - RMS error of the coil 2

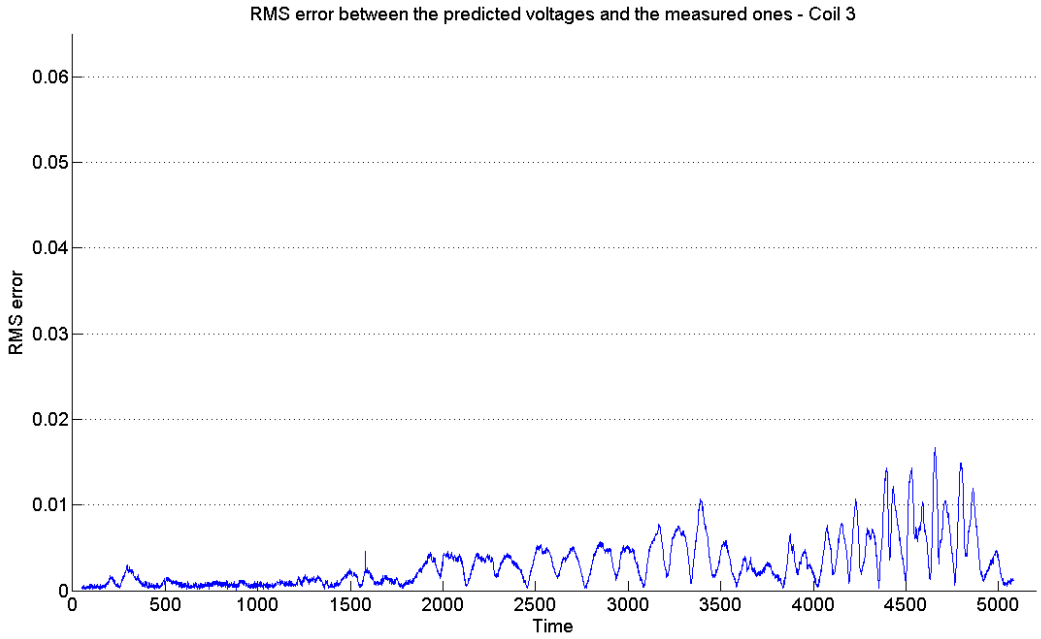

Figure 14 - RMS error of the coil 3

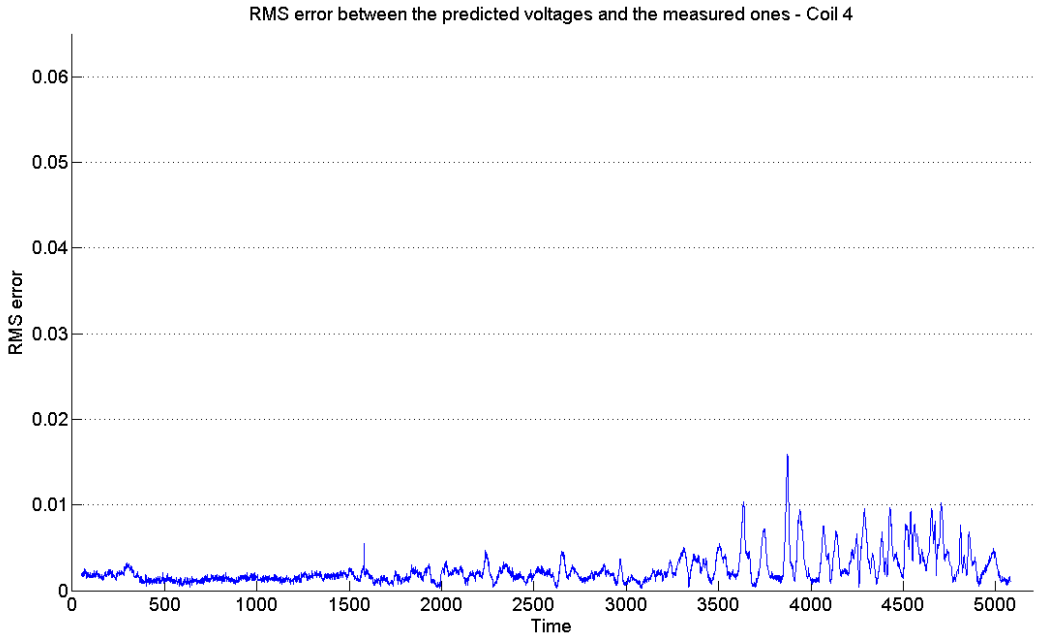

Figure 15 - RMS error of the coil 4

One can observe that the RMS error for the coil 2 is at least twice higher than for the other coils, which supports the hypothesis that there is still a “calibration” problem with the field model, inducing higher error when the axis of the coils are getting closer to the vertical axis.

4.4.1 Networks interpolating the voltages

Using the ANNs that were trained on the magnetic field, we ran the UKF algorithm to track each coil independently. Then, the distances between some of the coils were analyzed for every network. All the coils are fixed on the block. Therefore, when the coils are tracked independently using one of those networks, the trajectories of the coils should respect this constraint of moving the coils at the same distance.

Unlike the second coil, we know that the trajectories of the coils 3 and 4 are tracked coherently and with more satisfactory accuracy than the 2 others when the dipole model is used. In fact, they presented the smallest RMS error during this experiment (see Figure 12 to Figure 15). A good network used to track the coils independently should keep the distance between those 2 coils almost as constant as when the dipole model is used. One can observe in Table 6 that even the dipole model presents some inaccuracies and that the standard deviation of the distances between the coils 1 and 3, or the coils 3 and 4 is higher than 1 mm. Once again, this supports the idea of obtaining a new model for the magnetic field. However, Table 6 also shows that the *VoltNets* do not provide accurate tracking of the coil. Except for the Dual hidden-layered MLP networks with 50x400 hidden units, the standard deviation of the distances between two confident coils is superior to 2.5 mm, and the distances can deviate by more than 20 mm from their actual values.

ANN		calcamps	MLP	MLP DUAL	MLP DUAL	MLP DUAL	MLP DUAL	RBF RMQ	RBF RMQ
Hidden Units		N.A.	500	200x300	300x200	400x100	50x400	350	500
coil1-coil2	min	4.71	3.73	6.79	2.31	4.81	1.76	8.87	1.61
	max	73.88	51.78	42.27	74.74	62.07	521.66	351.99	283.21
	mean	20.09	30.68	22.30	20.94	22.95	30.39	149.76	106.14
	st. Dev.	5.91	8.92	4.31	7.62	5.45	61.37	87.77	99.49
coil1-coil3	min	41.51	37.60	36.49	42.91	43.71	53.54	28.76	28.44
	max	70.59	108.69	67.05	70.98	69.78	81.45	203.62	217.98
	mean	60.19	57.90	58.49	61.00	57.62	61.69	79.92	77.11
	st. Dev.	1.59	9.37	3.19	3.16	4.33	3.75	33.27	28.97
coil3-coil4	min	54.91	41.25	49.82	53.84	43.37	52.02	30.21	17.46
	max	62.74	68.86	70.73	69.15	67.78	63.90	81.05	142.45
	mean	59.90	61.31	57.89	61.50	60.86	59.32	59.86	65.00
	st. Dev.	1.20	5.07	2.53	2.52	4.93	1.76	8.03	17.09

Table 6 - Distances between coils using the VoltNets

In order to visualize those results, the distances between the coils 3 and 4 are plotted in Figure 16. This demonstrates that interpolating the voltages using those types of *VoltNets* does not provide satisfactory results. The computed distances with the coils tracked using those networks present many more spikes with higher amplitudes than with the dipole

model. Therefore, we can conclude that the voltages cannot be accurately interpolated using neural networks that are trainable with Matlab® and a training data set of 100,000 points.

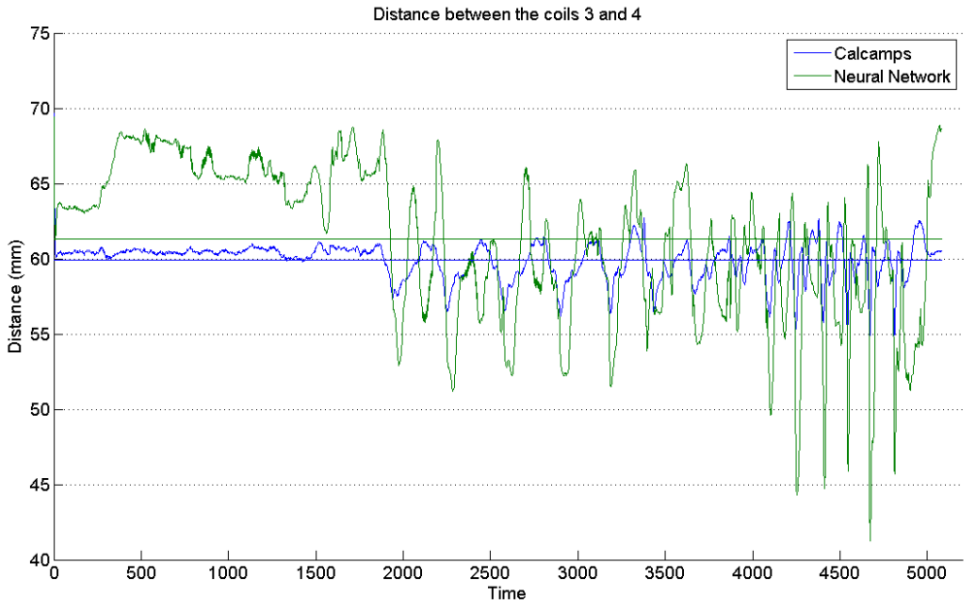

Single hidden-layered MLP Network with 500 hidden units

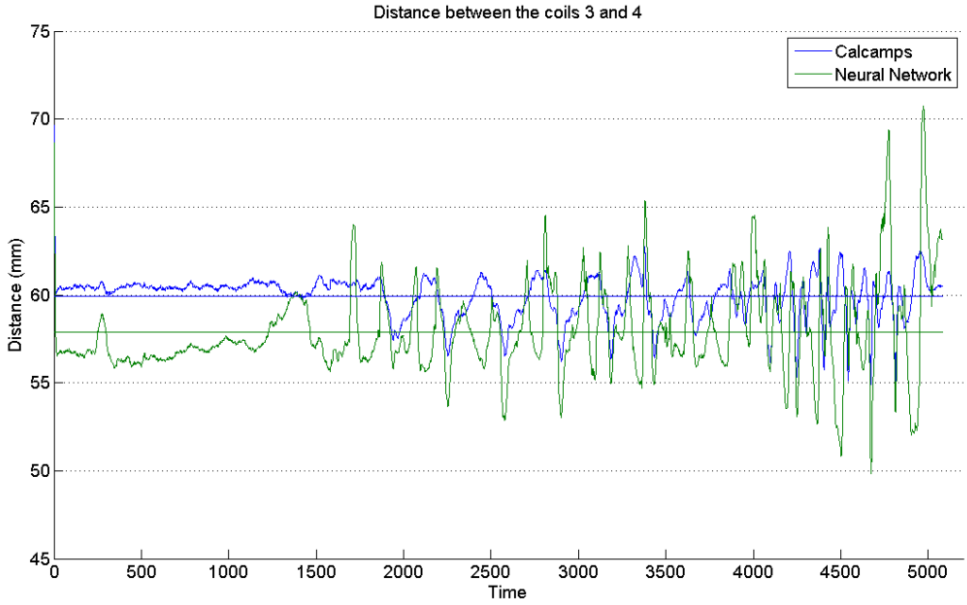

Dual hidden-layered MLP Network with 200x300 hidden units

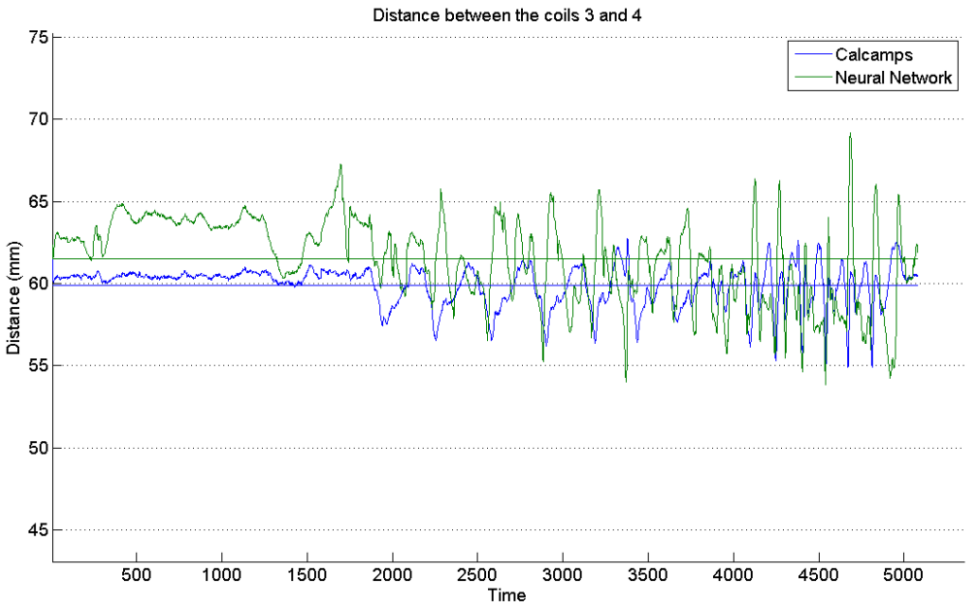

Dual hidden-layered MLP Network with 300x200 hidden units

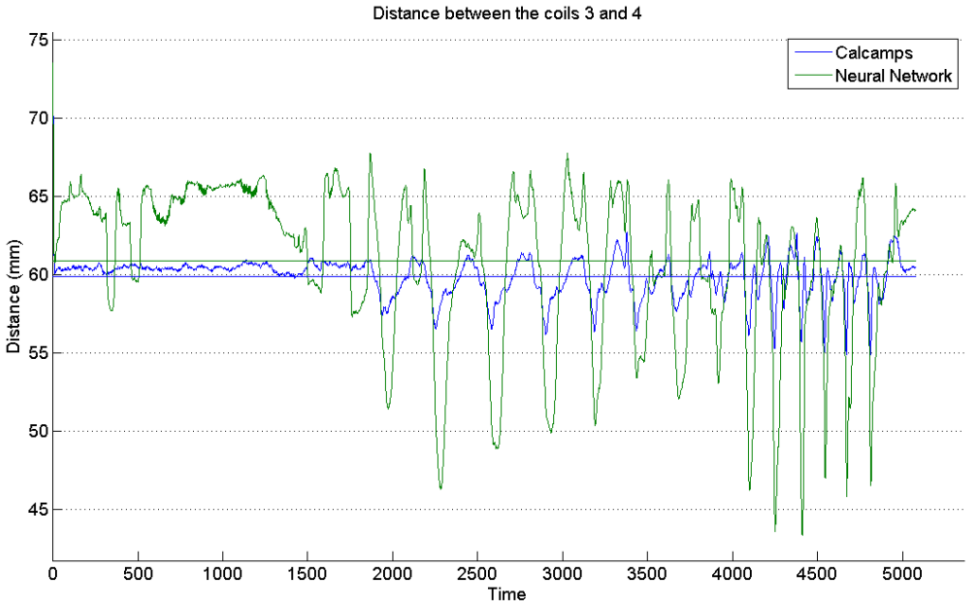

Dual hidden-layered MLP Network with 400x100 hidden units

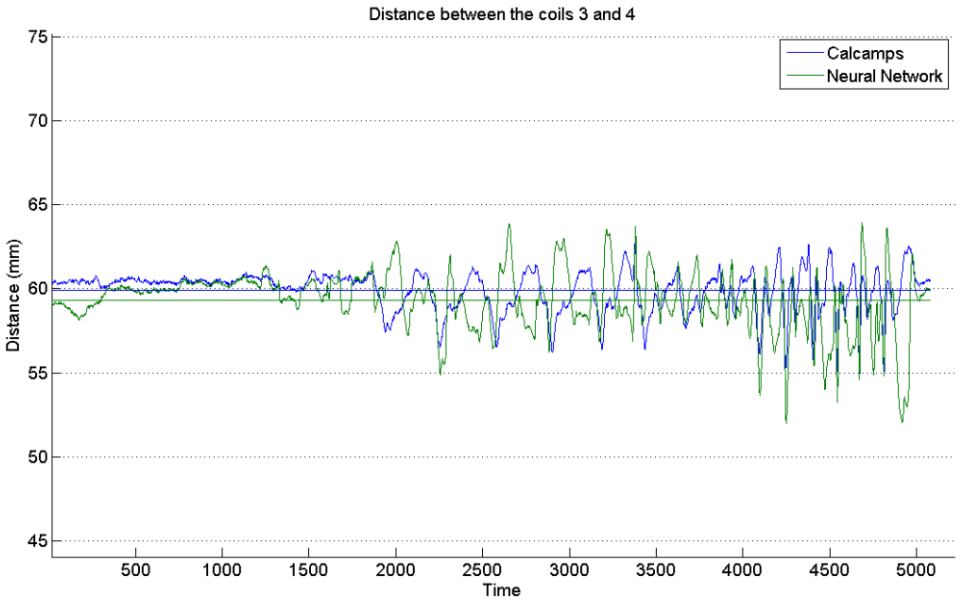

Dual hidden-layered MLP Network with 50x400 hidden units

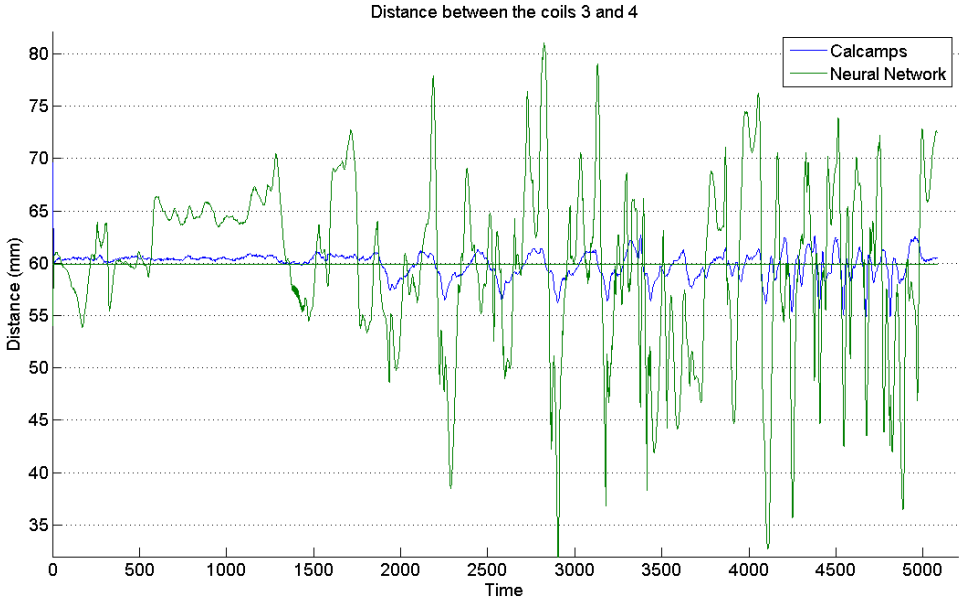

RMQ RBF Network with 350 hidden units

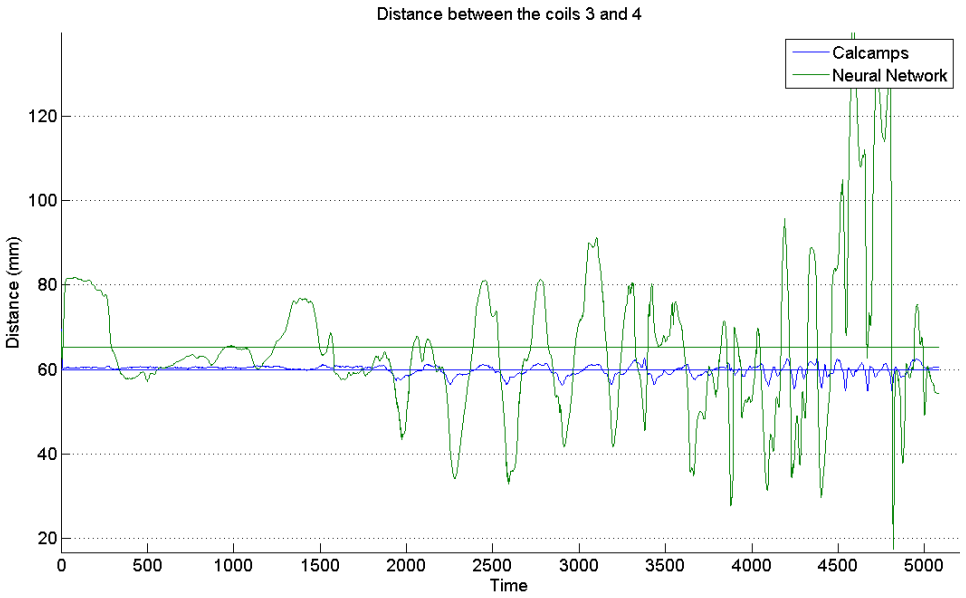

RMQ RBF Network with 500 hidden units

Figure 16 - Distance between coils 3 & 4 – VoltNets

4.4.2 Networks interpolating the magnetic field

In the same way as we evaluated the *VoltNets*, we used *FieldNets* to track the 4 sensors of the woodblock. The UKF algorithm was run with each of the ANNs. The results of these experiments (see Table 7) show that those *FieldNets* perform as well as the dipole model. The standard deviations of the distances between the coils 1 and 3, or the coils 3 and 4 are of the same order as the standard deviations obtained with the *calcamps* functions. The distances also range by the same amplitudes and the difference between the means of the distances is inferior to 0.3 mm.

ANN		calcamps	RBF RMQ	RBF Gaussian	MLP DUAL
Hidden Units		N.A.	350	500	30x30
coil1-coil2	min	4.71	4.69	4.63	4.85
	max	73.88	72.41	75.89	74.27
	mean	20.09	20.07	19.84	20.03
	st. Dev.	5.91	5.82	6.16	5.97
coil1-coil3	min	41.51	41.42	41.54	41.81
	max	70.59	70.78	72.42	70.78
	mean	60.19	60.20	60.00	60.23
	st. Dev.	1.59	1.61	1.76	1.63
coil3-coil4	min	54.91	54.92	55.00	54.84
	max	62.74	62.75	63.17	62.94
	mean	59.90	59.91	60.04	59.91
	st. Dev.	1.20	1.20	1.18	1.23

Table 7 - Distances between coils using the FieldNets

Those results show that the three *FieldNets* provide as accurate results as the *calcamps* function. Even the Gaussian Radial Basis Function network, which was not performing with the same accuracy on the validation set after the training, gives as satisfactory results as the other networks for this experiment. In order to visualize the performance, the distance between the coils 3 and 4 as a function of the time is provided below for each of the networks.

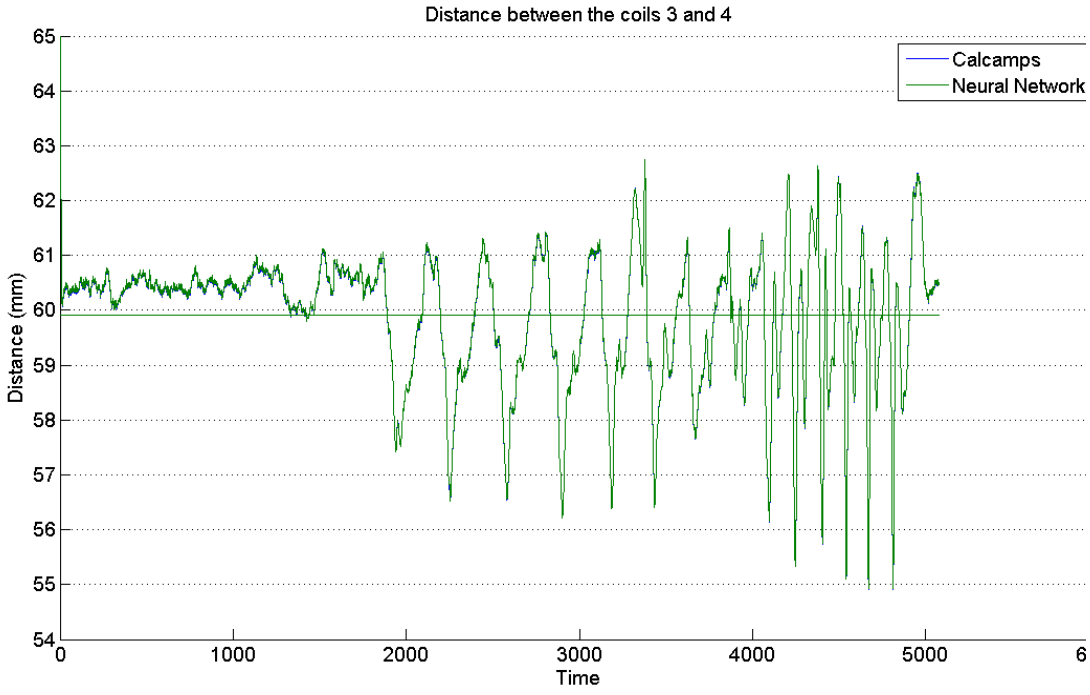

RMQ RBF Network with 350 hidden units

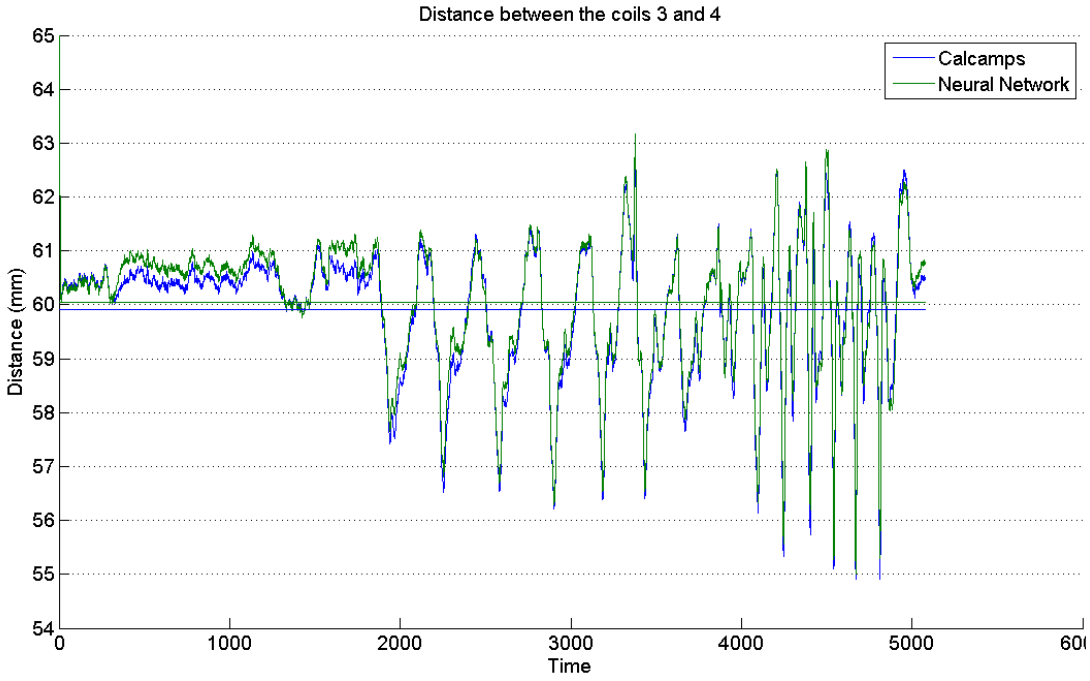

Gaussian RBF Network with 500 hidden units

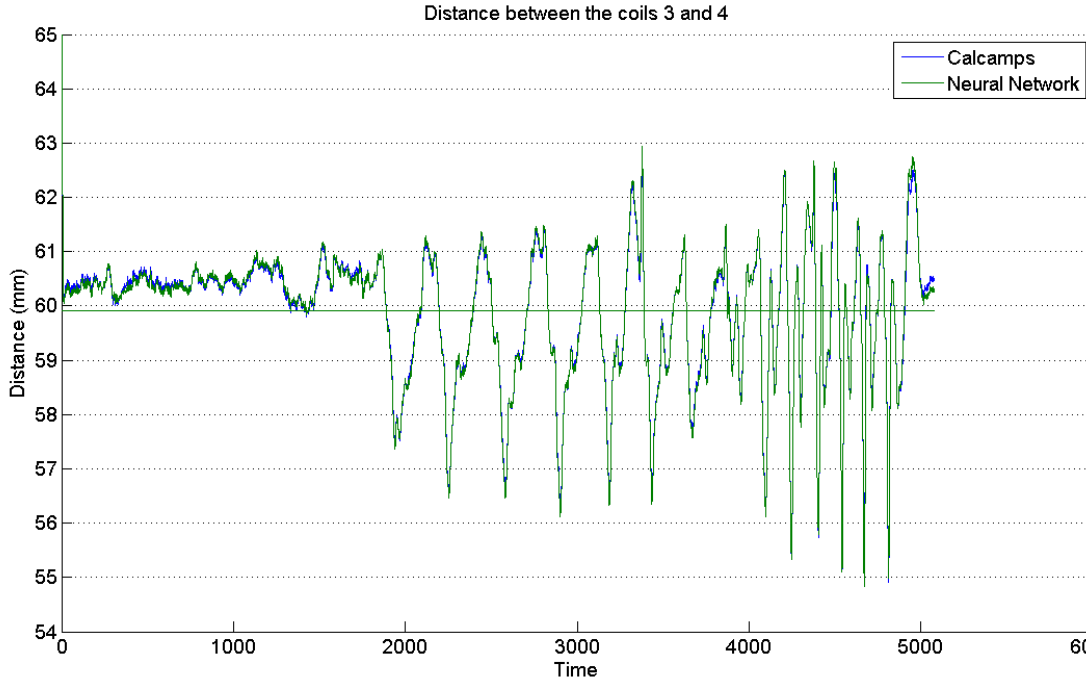

Dual hidden-layered MLP Network with 30x30 hidden units

Figure 17 - Distance between coils 3 & 4 - FieldNets

Those plots show that these networks provide results that are similar to the ones obtained with the *calcamps* function. The Reverse hardy's Multi-Quadrics network with 350 hidden neurons computed a distance between the coils 3 and 4 that almost perfectly matches the distance computed with the dipole model. The distances tracked with the two other networks are also quite similar to the ones tracked with the *calcamps* function. Therefore, this provides evidence that the magnetic field vector can be interpolated with a **trainable** model.

Chapter 5 Optimizing the field model

5.1 A constrained tracking problem

In order to optimize the field model initialized from the dipole model (as in Chapter 3), some more data are necessary so that the field model can be adjusted. Some perturbations due to the environment can slightly modify the magnetic field and therefore add some error to the tracking process. The aim of the field model optimization is to obtain a function that is closer to the actual magnetic field or the actual amplitude of the voltages to make up for those perturbations. The only way of doing this kind of optimization is to measure some data to get some knowledge about the actual magnetic field. One way of doing this is to record the voltages with some sensors moving through the field. However, in order to get data that provide information about the relationship between the state of the coils and the measured voltages, one needs to have some precise knowledge about the position and the orientation of some coils.

In this project, we propose an alternative approach based on a constrained tracking problem. Several sensors were fixed relative to each other on a rigid block and moved through the measurement space. Thus, the positions and the orientations of the coils relative to each others remain fixed although none of the trajectories is known accurately. Working out how best to exploit this knowledge of the fixed distances is not trivial. For example, if 2 coils are fixed relative to each other at a distance D, knowing the state of one of them does not define the position of the second coil. The latter could be anywhere on the surface of the sphere of a radius D, centred at the first coil. Adding the information of the tracked trajectory of the second coil does not even define exactly its position given that the tracked one could even not be on the surface of this sphere. Given that we do not know exactly the position of either of the 2 coils, the difficulty is even higher.

To tackle this problem, we implement a solution which is based on an Unscented Kalman Filtering algorithm . We use the data from the woodblock with the 4 coils. Then, assuming that the coils 1, 3 and 4 are reliable enough (see section 4.4), the constraints between the sensors are used along with an Unscented Kalman Filter to enhance the accuracy of the tracking process.

The implementation of such a method is different from the one that was used to track the coils independently. The state variable is no longer the 5-dimensional state of the coil but a 6-dimensional vector that describes the state of the whole block onto which the coils have been fixed. These six degrees of freedom are the 3 Cartesian coordinates and the 3 orientation angles of the block that have been chosen to be the Euler angles. Those angles, α, β and γ, represent the rotation around the z-axis, the line of nodes axis and the new Z-axis respectively (see Figure 18). The line of nodes axis is the intersection of the xy plane before rotation of the coordinate system, and the plane XY after the rotation.

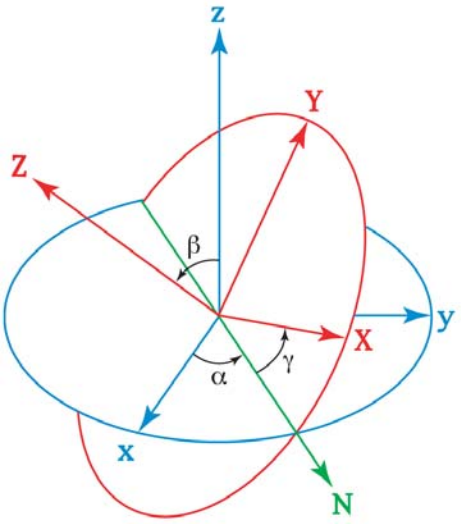

Figure 18 - Euler Angles
(Figure from http://en.wikipedia.org/wiki/Euler_angles)

The state transition model is still set with the identity matrix, and the transition equation includes some process noise with a zero mean multivariate distribution, as described below:

$$\begin{bmatrix} X_k \\ Y_k \\ Z_k \\ \alpha_k \\ \beta_k \\ \gamma_k \end{bmatrix} = \begin{bmatrix} X_{k-1} \\ Y_{k-1} \\ Z_{k-1} \\ \alpha_{k-1} \\ \beta_{k-1} \\ \gamma_{k-1} \end{bmatrix} + w_{k-1}$$

where $\begin{bmatrix} X_k \\ Y_k \\ Z_k \\ \alpha_k \\ \beta_k \\ \gamma_k \end{bmatrix}$ are the coordinates of the block at time k, and w_k is the process noise

The measurement equation is more different from the previous model that was used to track the coils independently. The measurements are all the voltages recorded with every coil that has been fixed on the block. Knowing with some confidence the positions and the orientations of every coil on the rigid body, the state of the block at time k can be linked to

the whole set of the recorded voltages, which exploits the knowledge of the constraints between the coils. The measurements also include some observation noise, as described below:

$$\begin{bmatrix} V_{1,1_k} \\ \vdots \\ V_{1,6_k} \\ V_{2,1_k} \\ \vdots \\ V_{n,6_k} \end{bmatrix} = f\left(\begin{bmatrix} X_k \\ Y_k \\ Z_k \\ \alpha_k \\ \beta_k \\ \gamma_k \end{bmatrix}\right) + v_k$$

where:

- V_{i,j_k} is the j[th] voltage measured on the i[th] coil at time k, where n is the number of coils fixed on the block,
- f is the observation model based on the position of the sensors relative to the position of the block, and the field model,
- v_k is the observation noise which is assumed to be zero mean Gaussian white noise.

The observation model f uses either the dipole model, or one of the *FieldNets* trained in section 3.3.3. Given the arrangement of the coils on the block, the position and the orientation of each of them can be inferred from the state of the block, and then linked to the voltages. A more precise description of this is provided in the following section.

5.1.1 Tracking the woodblock in the field

The coils on the woodblock were placed with different orientations and different distances. Figure 19 illustrates the relative positions of the coils and shows how the local coordinate was chosen to link the 6 coordinates of the block to the coordinates of each of the coils. The 3[rd] coil was chosen to be the origin of the local coordinate system.

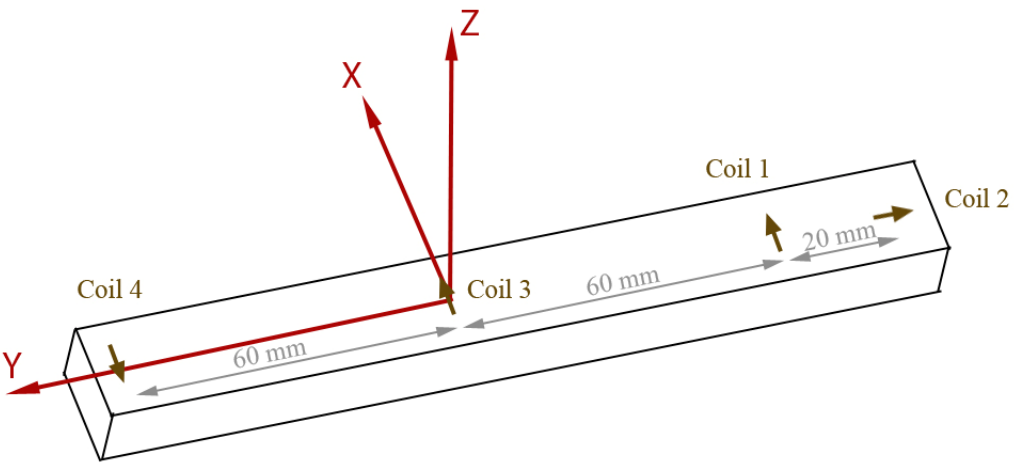

Figure 19 - Woodblock with 4 coils and the local coordinate system

The intended positions of the coils in the local coordinate system are summarized in Table 8.

Coil	X (mm)	Y (mm)	Z (mm)	θ (degree)	φ (degree)
1	0	-80	0	0	0
2	0	-60	0	-90	0
3	0	0	0	0	0
4	0	60	0	180	0

Table 8 - Intended local positions of the coils on the woodblock

Given these local coordinates of the coils and the global coordinates of the woodblock, it is then possible to compute the global coordinates for every coil. This local coordinate system is obtained from the global coordinate system with a composition of rotations, which have been chosen to be the Euler rotations. Given the three Euler angles, the matrix representations of the rotations were multiplied with the vectors of the local coordinates of each coil to obtain the positions in the global coordinate system. The orientation of each coil was converted into three Cartesian coordinates to allow the multiplication with the rotation matrices. The three Euler rotations were represented as follows:

$$Rz = \begin{bmatrix} \cos(\alpha) & -\sin(\alpha) & 0 \\ \sin(\alpha) & \cos(\alpha) & 0 \\ 0 & 0 & 1 \end{bmatrix}$$

$$Rn = \begin{bmatrix} 1 & 0 & 0 \\ 0 & \cos(\beta) & -\sin(\beta) \\ 0 & \sin(\beta) & \cos(\beta) \end{bmatrix}$$

$$RZ' = \begin{bmatrix} \cos(\gamma) & -\sin(\gamma) & 0 \\ \sin(\gamma) & \cos(\gamma) & 0 \\ 0 & 0 & 1 \end{bmatrix}$$

where:

- Rz is the rotation around z-axis the global coordinate system,
- Rn is the rotation around the line of node,
- RZ' is the rotation around the Z-axis of the rotated frame.

The coordinates of each coil in the global coordinate system are computed as follows:

$$\begin{bmatrix} x \\ y \\ z \\ x_o \\ y_o \\ z_o \end{bmatrix} = Rz\ Rn\ RZ' \begin{bmatrix} X \\ Y \\ Z \\ X_o \\ Y_o \\ Z_o \end{bmatrix}$$

where the coordinates in the local frame are in capital letters, the ones in the global coordinate system in small letters, and where the variables with a subscript "o" denote the Cartesian representation of the unit vector of the orientation.

Given the positions and orientations in the global coordinate system, the corresponding voltages can be calculated with either one of the *FieldNets*, or the *calcamps* function from the TAPADM toolbox. This relationship between the state of the woodblock and the measured voltages constitutes the observation model used in the unscented Kalman filter.

Given that the Euler angles are defined modulo 2π, we had to use the option available in the Rebel toolbox to deal with angle discontinuities. This was set by adding the following line of code:

```
model.stateAngleCompIdxVec = [4 5 6];
```

This line declares the parameters number 4, 5 and 6 as angles before the Inference data structure is created in Rebel.

5.1.2 Several alternatives to track the woodblock

Previous analysis (section 4.4) has shown that some parts of the tracked trajectory of the coil 2 on the woodblock present some irregularities. When the axis of this sensor is close to the z-axis of the global coordinate system, the tracked position of this coil deviates distinctly from its actual one that we can approximately infer from the positions of the 3 other sensors. Therefore, when the Unscented Kalman filtering algorithm is run to track the trajectory of the woodblock, this coil gives erroneous information that might add some error to the

tracked movement. In order to gauge the impact on the tracking process, we implemented two versions of the measurement equation in the UKF. In a first experiment, the 24 voltages that correspond to the 4 coils were used to define the observations for the model, and in a second experiment, the coil n°2 was excluded from the model to use only the 3 other coils. In the latter version, only the 18 voltages corresponding to the exploited coils were taken into account.

Then, we used the trajectories of the 4 coils tracked independently with the *calcamps* function to do further analysis. Given the tracked positions and orientations of the block, we applied the opposite rotations and translations to the independent trajectories of the 4 coils in order to observe their local movement in the local frame of the woodblock. This was done for both the experiment using the 18 voltages and the one using the 24 voltages. The plots in Figure 20 to Figure 25 represent the local Cartesian coordinates of the coils in the frame of the woodblock.

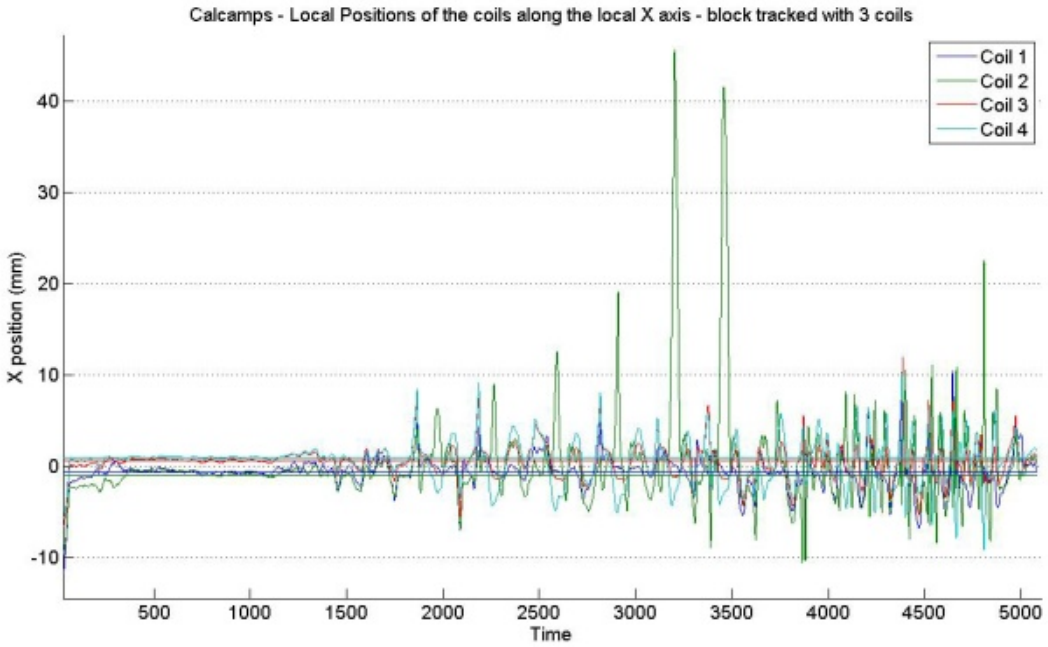

Figure 20 - Local positions on X-axis - Block tracked with 3 coils

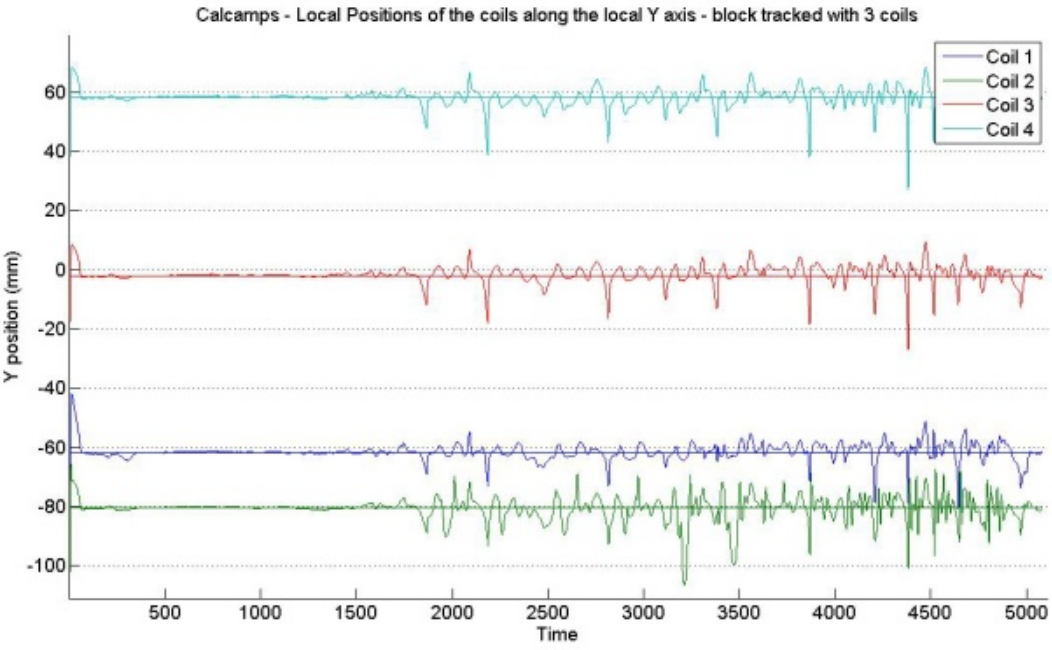

Figure 21 - Local positions on Y-axis - Block tracked with 3 coils

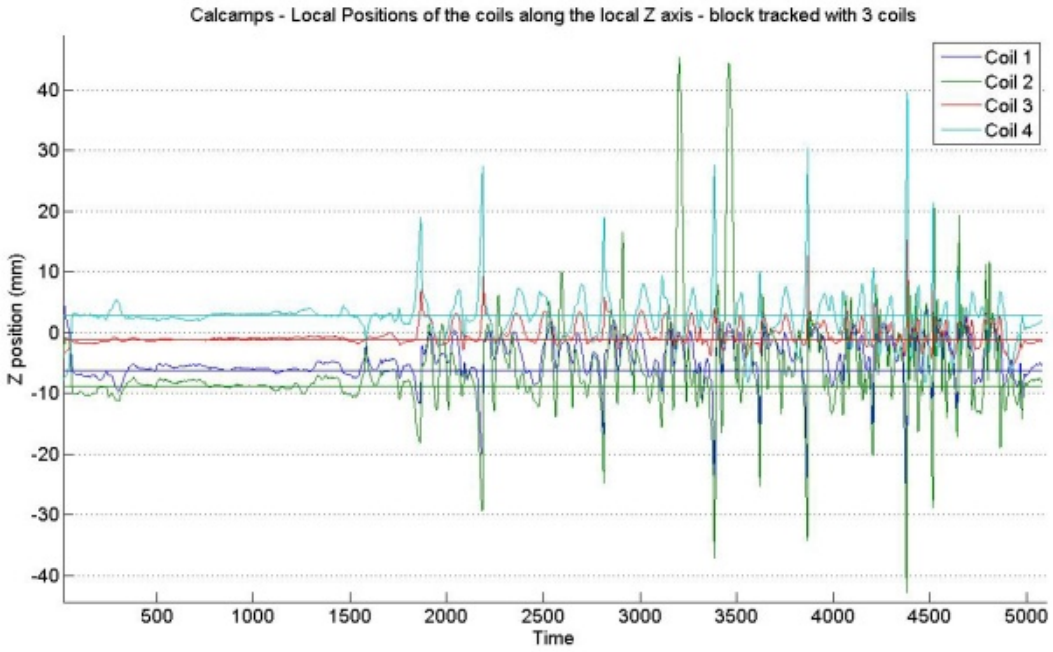

Figure 22 - Local positions on Z-axis - Block tracked with 3 coils

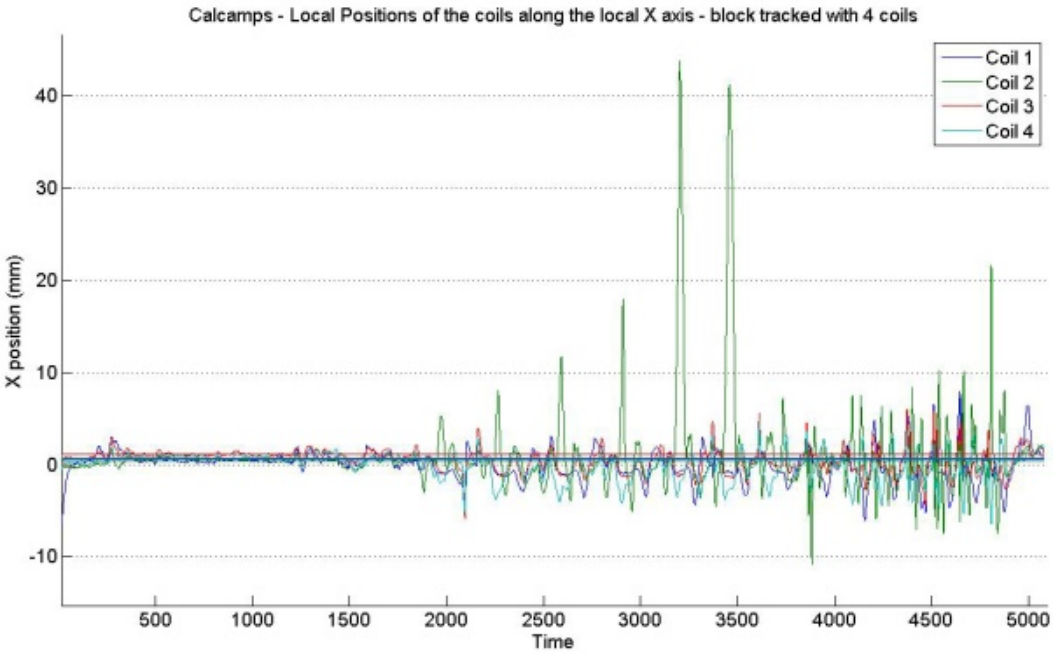

Figure 23 - Local positions on X-axis - Block tracked with 4 coils

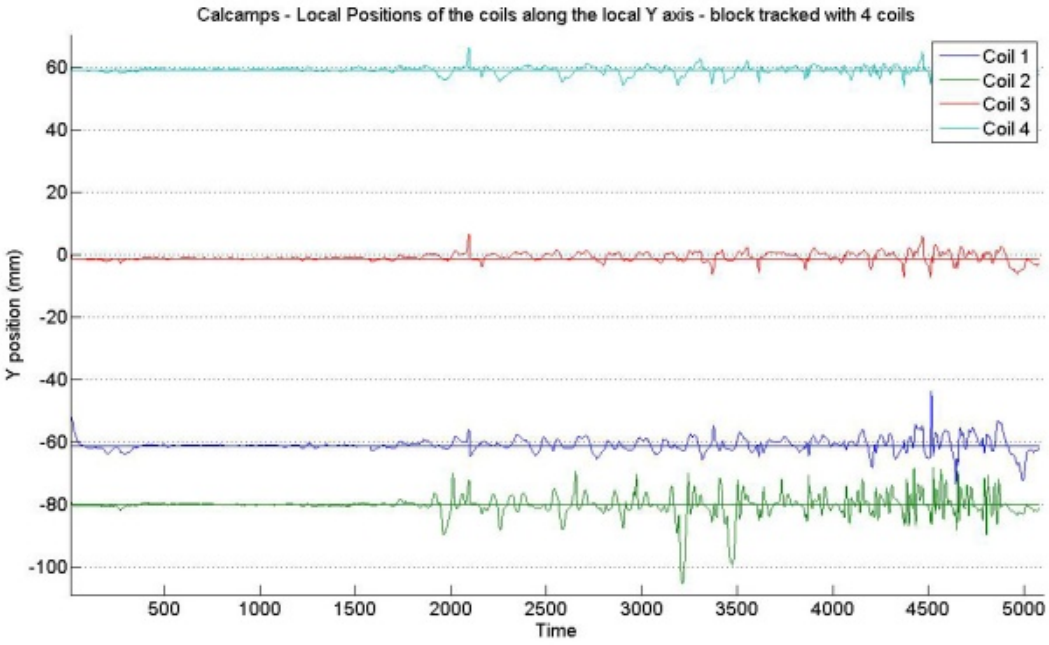

Figure 24 - Local positions on Y-axis - Block tracked with 4 coils

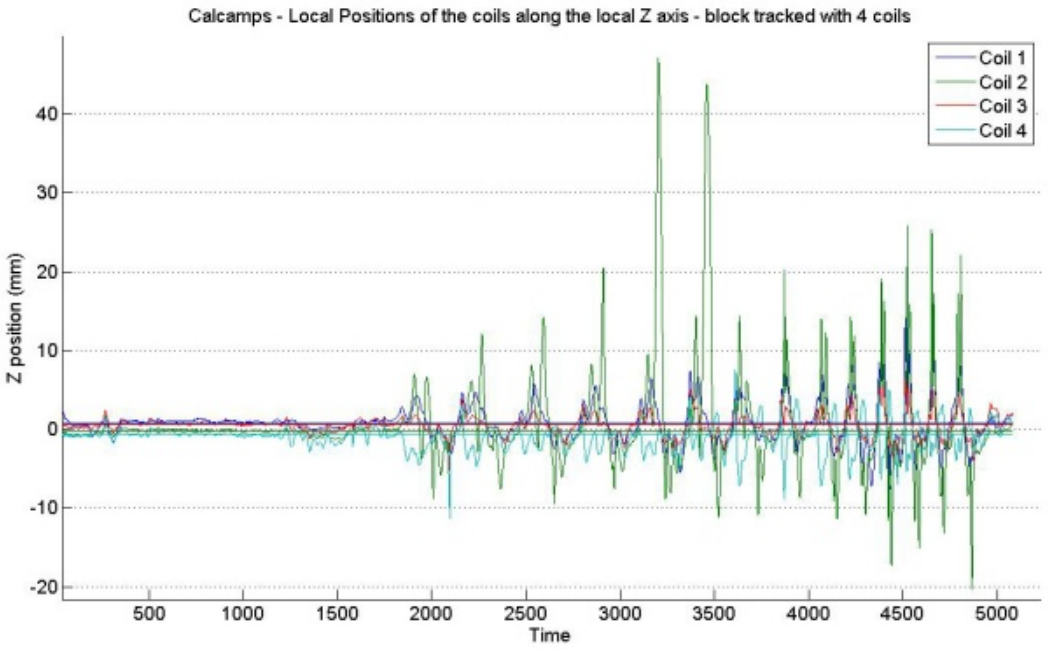

Figure 25 - Local positions on Z-axis - Block tracked with 4 coils

The coils were stuck on the woodblock with the intended positions and orientations given in Table 8. There might be some slight deviations from those which could be about 1

mm and a couple of degrees. This could be the cause of a small difference from the 0-axis that one can observe in Figures Figure 20, Figure 22, Figure 23 and Figure 25. However, this small error should be in the order of 1 mm for the Cartesian coordinates and 2 or 3 degrees for the angles. Even if the tracked trajectories of the coils are not the actual ones, we know that the local movements in the frame of the woodblock should stay around the intended locations reported in Table 8. The positions of the coils in the local frame when the block was tracked with 3 coils present a higher deviation from the intended values than when the block was tracked with the whole set of coils. This can be observed distinctly with the X and Z local coordinates. In Figure 22, the difference can be up to 10 mm on the Z-axis. The coil 4 stays around +5 mm on this axis, and the coil 1 around -5 mm, while both of them should stay in the local XY plane. As a matter of fact, the remaining constraints when only 18 voltages are processed to infer the state of the woodblock are not sufficient. Given that there are fewer constraints, the orientations of the main axis of the woodblock (which is the local Y-axis) are tracked with lower precision. The calculated orientations of this axis differ from the actual ones and the coils are no longer in the local XY plane, which explains this difference in the positions on the Z-axis.

Therefore, the tracking algorithm that exploits the 24 voltages is more appropriate for this problem, even if the trajectory of the second coil presents some irregularities. The version of the constrained tracking is the one that has been retained.

5.2 An EM approach to optimize the tracking of the woodblock

The field model currently in use allows tracking the coils with an error which is below 1 mm. In order to expect any improvement of this model using measured data, one must utilize reliable data so that the optimization of the model will not degenerate to nonsense. With the solution of the constrained tracking, the relative positions and orientations of the coils must be known with high confidence. However, the “theoretic” arrangement of the coils on the woodblock might slightly differ from the actual ones. Given that these data are supposed to be analyzed to optimize the field models, they must be precise and reliable for this purpose. Therefore, the relative positions used need to be processed and optimized to make those new limited training data as accurate as possible and to expect some improvement of the field model.

5.2.1 Measuring the positions and orientations of the coils on the woodblock

There are many different ways to try to discover the relative positions of the coils on a block. However, the difficulty to achieve this optimization is that each coil has 5 degrees of freedom which, added to the 6 degrees of the freedom of the block, makes a challenging number of unknowns. Therefore, in order to make up for this high dimensionality of the space where the optimization is computed, one needs to either use more equations, either keep some constraints. The first option would require more measures for the coils, which means more voltages, and which is then not conceivable. The second option can be done by assuming that we have some knowledge about the relative positions and orientations of the coils. This presumably correct knowledge should be defined according to the problem.

Regarding the woodblock, there are different variables describing the states of the coils on the woodblock that could be assumed to be known with a high confidence. Some others can be potentially less confident, and these are the variables that we want to refine. On the block, the coils are supposed to be perfectly aligned. Given the distances between the coils, one can assume that this alignment is sufficiently correct. However, the distances could present a small inaccuracy, and given that they are supposed to be utilized in the observation model to track the whole block, their actual values should be known with high confidence.

In order to discover the distances, those were introduced as unknown in the Unscented Kalman filtering algorithm, even if they are still parameters in the observation model. Doing that, the tracking algorithm becomes an alternative version of the UKF, called the Joint Unscented Kalman Filter. This version of the algorithm optimizes jointly the unknown variables and parameters, i.e. it tracks the block and optimizes the distances used in the observation model at the same time.

The difficulty that was encountered is that the distances are actually a function of the 3 Cartesian coordinates of the coils, which means that knowing the distances between the coils does not give sufficient knowledge about their relative positions. A coil situated at a known distance from another could be anywhere on the surface of the sphere centred on the second coil with this distance as radius. Therefore, we had to assume that the coils were confidently aligned on the block. Therefore, the distance was expressed by the position on the local Y-axis (see Figure 19). The augmented state vector of the Joint Unscented Kalman Filter was defined as follows:

$$Joint\ State = \begin{bmatrix} X \\ Y \\ Z \\ \alpha \\ \beta \\ \gamma \\ D_1 \\ D_2 \\ D_4 \end{bmatrix}$$

where X, Y, Z, α, β and γ describe the state of the woodblock as defined in section 5.1, and D_1, D_2 and D_4 describe the distances of the coils 1, 2 and 4 respectively, from the coil 3 which was chosen to be the origin of the local coordinate system. This augmented state contains the distance parameters which are optimized jointly with the positions and orientations of the block. In the observation model, the optimized distances were used as the coordinates of those 3 coils on the local Y-axis.

The joint UKF was run on the same data set of the woodblock. The variance of the noise corresponding to the distances was set to a small value (10^{-7}), given that they are not supposed to vary significantly. The results are reported in Figure 26.

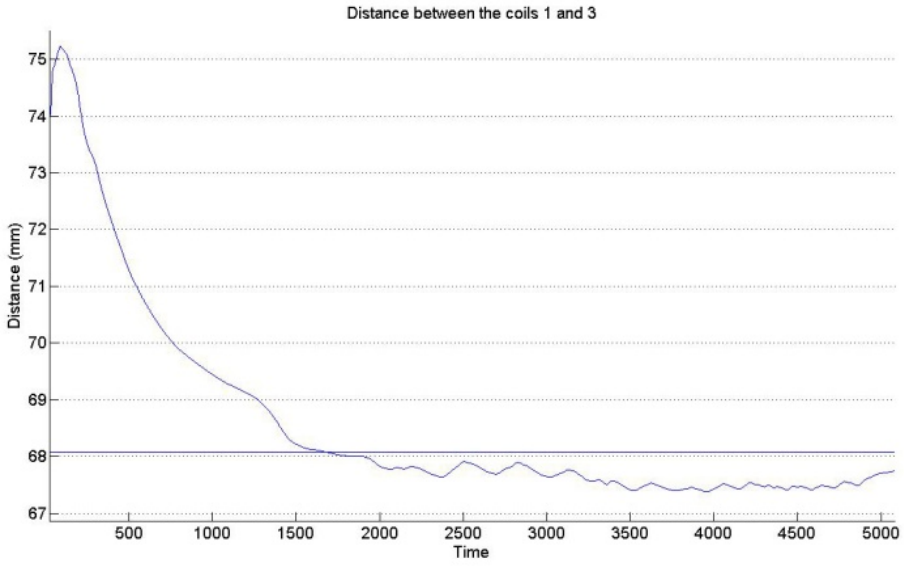

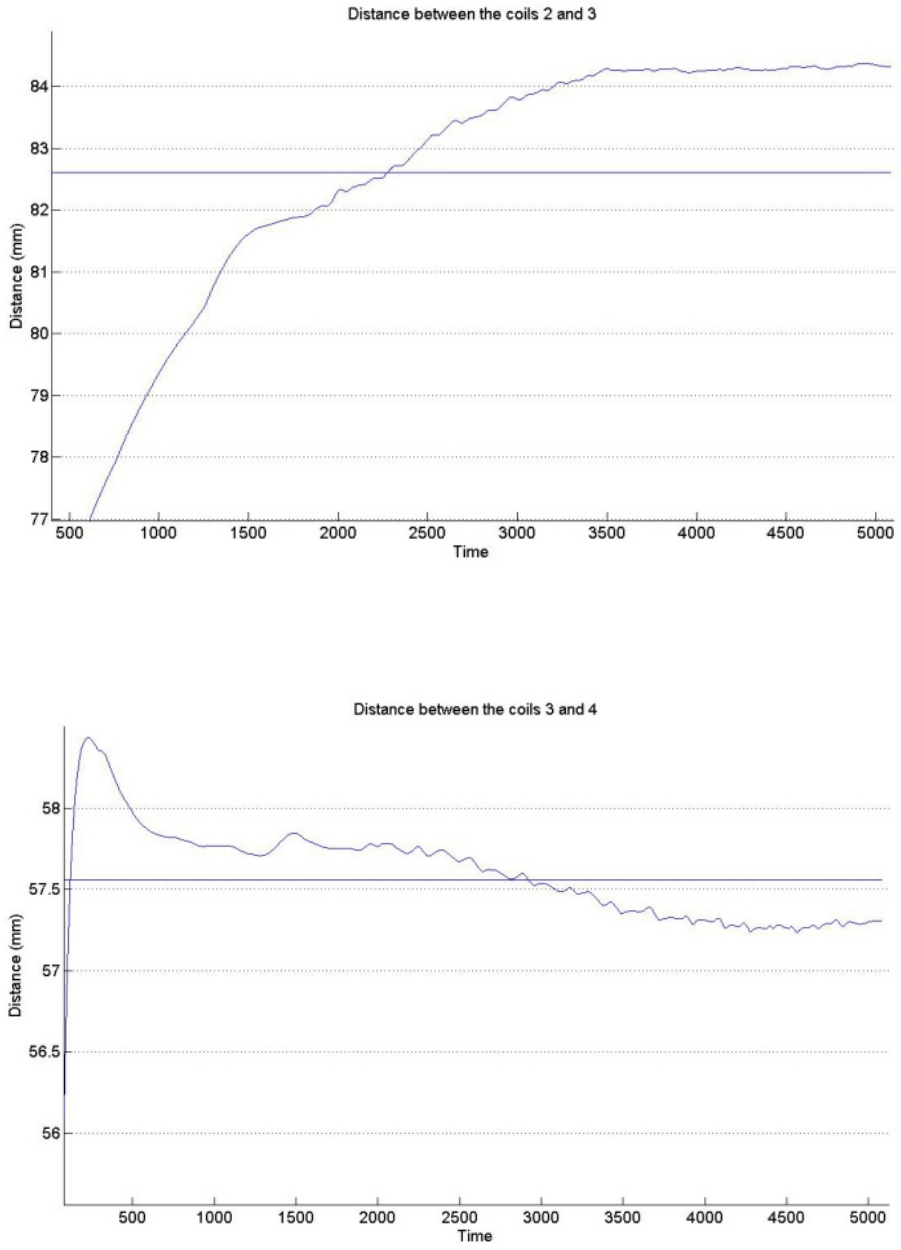

Figure 26 - Optimization of the distances between the coils

	Coil 1 to Coil 3	Coil 2 to Coil 3	Coil 3 to Coil 4
Mean distance (mm)	68.07	82.61	57.56

Table 9 - Mean of the optimized distances

This solution presented bad results. In fact, the coils are supposed to be fixed on the woodblock at positions and orientations close to the intended ones (see Table 8) and should not differ from them by more than 1 or 2 mm regarding the Cartesian coordinates. Therefore,

we wanted to assess if the problem was not a consequence of a bad tracking of the block. Given the distances and the state of the block tracked jointly, the global positions of the coils were computed. Then, given those global positions and orientations of the coils, we took back the movement of the block tracked with 4 coils and the *calcamps* function and we evaluated the trajectories of the coils in this local frame. The evolutions of the local coordinates of the coils are plotted in Figure 27.

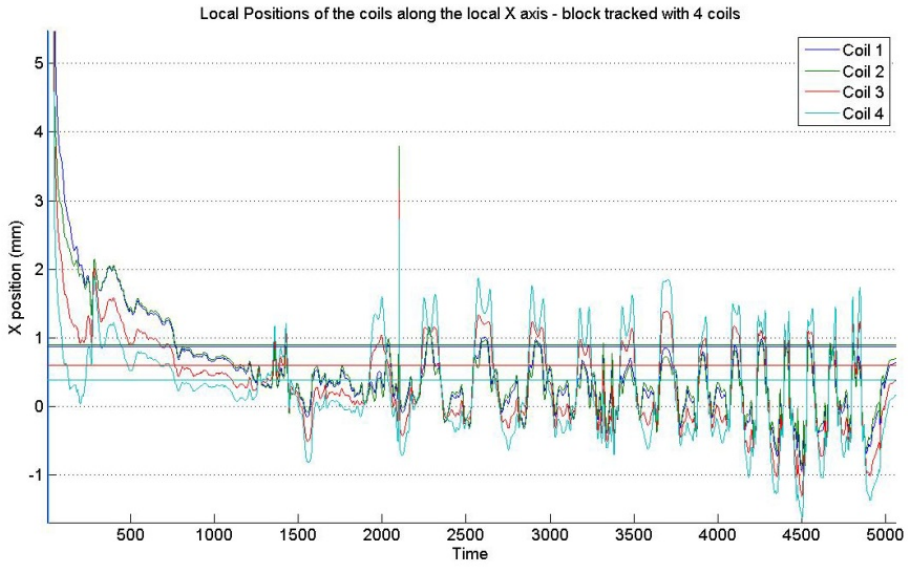

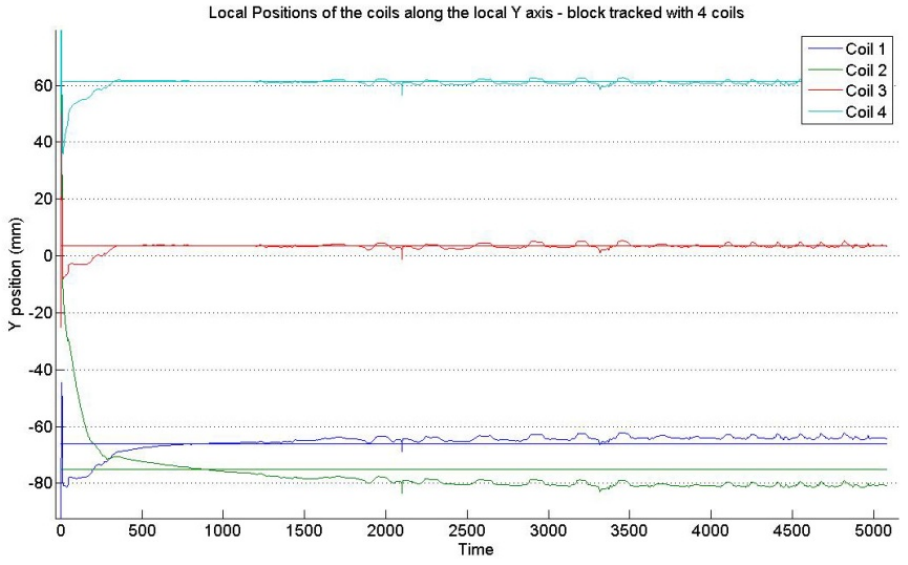

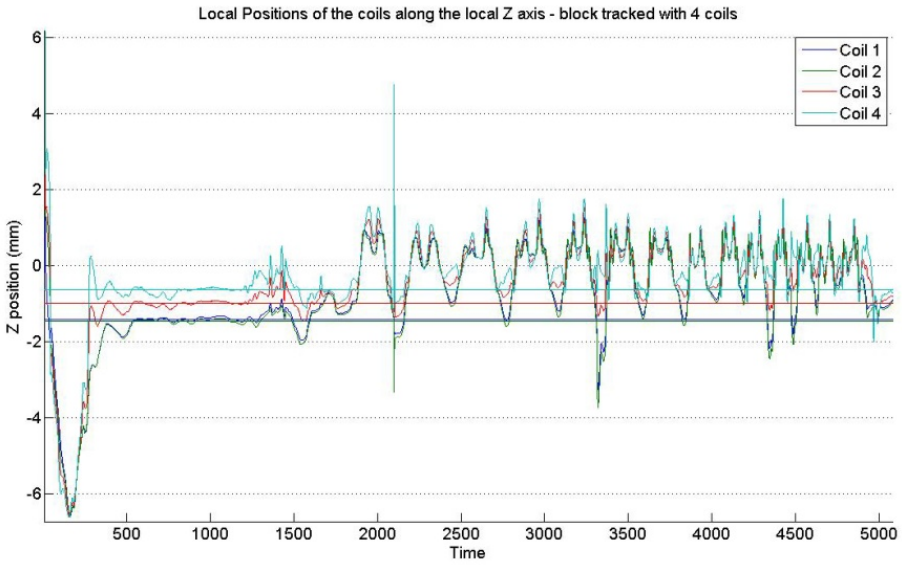

Figure 27 - Local positions of the coils while distances are optimized

In Figure 27, we can observe that the local coordinates are not as incorrect as the distances were. In fact, the difference with the intended values stays below 2 mm, which is much more satisfactory than the results obtained for the distances, i.e. the Y Cartesian coordinate in the frame of the woodblock tracked jointly. Therefore, we can provide some explanations to these results. First, the movements of the coils in the local frame of the woodblock tracked with *calcamps* show that the overall tracking process has not degenerated to nonsense. The trajectory of the coils is still sensible with respect to the ones calculated in section 5.1.2. However, we can infer that the trajectory and in particular the orientation of the block is no longer followed accurately, which could explain the divergence of the positions on the local Y-axis. When we reconstituted the movements of the coils using the jointly optimized woodblock trajectory and parameters, we could observe that these reconstituted movements were similar to the ones obtained in section 5.1.2. This provides some evidence that these inaccuracies compensate each other. Secondly, the Joint UKF algorithm used an augmented state, which added some degrees of freedom to the problem. This might be one of the causes of this divergence of the distances, as well as this was observed with the comparison in section 5.1.2 when the block was tracked with 3 coils. Thirdly, the assumption that the coils where perfectly aligned might also induce some error and cause this divergence.

Some other ways of optimizing the parameters were tested. Firstly, we added more degrees of freedom to the augmented state. The 6 variables describing the state of the woodblock were augmented with the 15 variables that depict the local state of the coils 1, 2

and 4 in the local frame. For those 3 coils, the 3 Cartesian coordinates and the 2 angles were added to the state to optimize their arrangement with a Joint Unscented Kalman filter. This made a 21-dimensional joint state composed of 6 variables for the state of the woodblock and 15 parameters. In order to evaluate the results, we plotted the evolution of the local Cartesian coordinates (Figure 28).

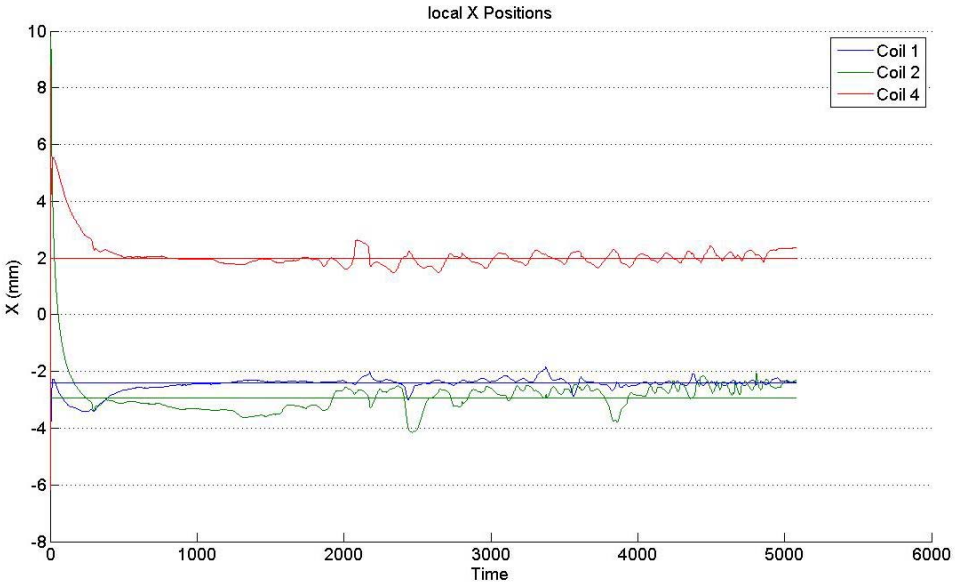

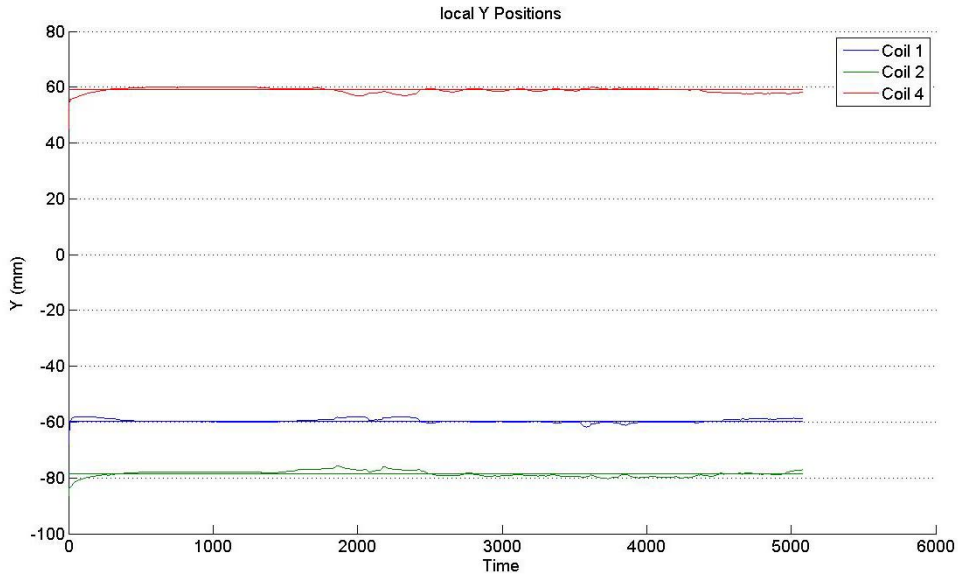

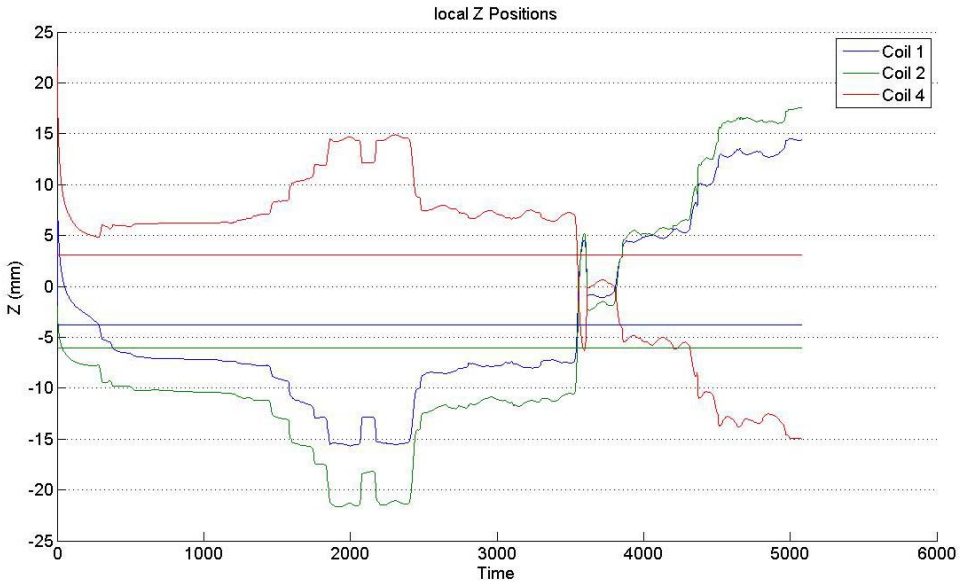

Figure 28 - Jointly optimized local positions

We observe (2nd plot) that the values of the local Y-coordinate stay close to the intended ones, with some variations though. However, the local Z-coordinates (3rd plot) vary quite randomly around the 0-axis. Nevertheless, one can notice that the position of the coil 4 on this axis presents some symmetry with the positions of the coils 1 and 2 somehow. Given that the coil 4 is supposed to be in the positive values of the Y-axis and the 2 others in the negative values, this symmetry suggests that this "random" behaviour along the Z-axis might be a consequence of some inaccuracy in tracking the Euler angles defining the orientation of the block. These 2 inaccurately tracked variables compensate each other, ensuring a coherent movement of the coils in the global coordinate system.

Secondly, we slightly modified this previous model to try to increase the constraints on the axis where the coils are supposedly aligned. Therefore, we considered as parameters the 8 angles corresponding to each of the 4 coils, the distance between the coils 1 and 3, and the 3 local Cartesian coordinates of the coils 2 and 4. This ended up with an augmented joint state-parameter vector of 21 variables: 6 variables describing the state of the block augmented with the 15 variables cited above. After running the Joint UKF algorithm, we observed that this model did not provide satisfactory results and that it was not adequate for this problem. For example, the distance between the coils 1 and 3 should remain around the intended value of 60 mm. Figure 29 shows that the tracked distance does not satisfy this criterion.

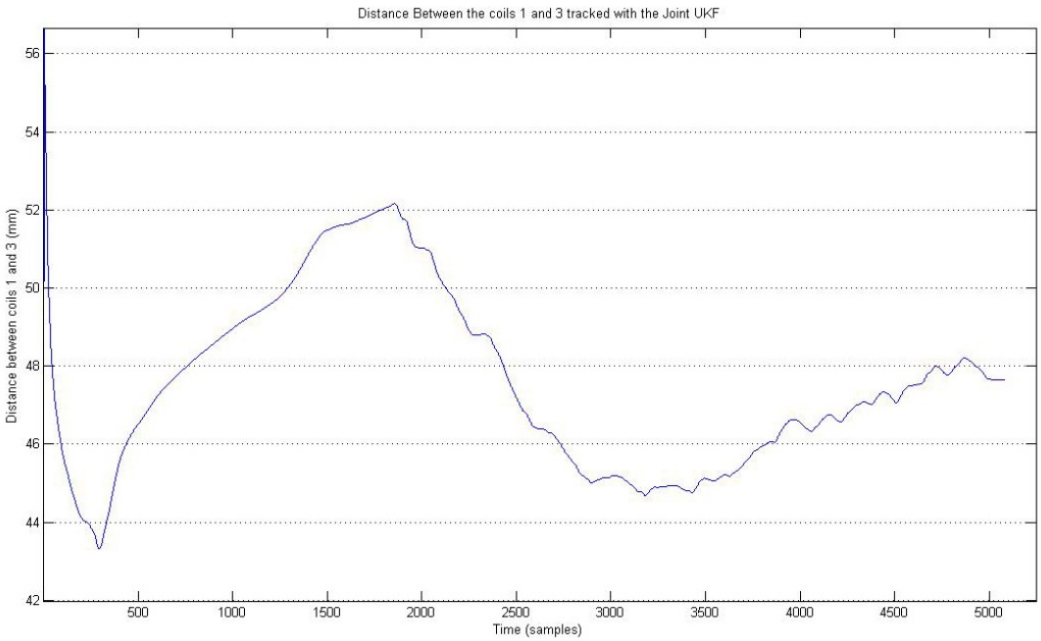

Figure 29 - Distance between the coils 1 and 3 tracked with the Joint UKF

Those experiments show that the optimization of the relative positions and orientations of the coils is quite challenging. There might be some explaination to this problem. Only 4 coils were fixed on the block. The amount of available data on the block might not be sufficient and therefore, when the state is augmented with the parameters, the tracking algorithm encounters a lack of information. The solid block is then tracked with a lower accuracy which, with the woodblock, was expressed by the erroneous Euler angles.

Chapter 6 Conclusion

6.1 Summary of the project

Electromagnetic Articulography has caught the curiosity and the interest of many scientists. Its applications are numerous and this might be adapted to create many new technologies. The AG-500 is one of the most sophisticated and developed device used in research in this field. It is superior to the 2-dimensional predecessors (AG-100 and AG-200) because of the light sensors allowing all kind of movements and because it provides 3-dimensional tracking in 5 degrees of freedom. It is expected to measure the sensor positions and orientations with a smaller error than its predecessors. However, the measurement principle relies on an inaccurate model of the magnetic field, which is quite sensitive to perturbations. Therefore, some measurement errors could be reduced if the magnetic field model was adapted to true physical one where the experiments are done.

In this project, we wanted to test and evaluate the potential to interpolate the magnetic field or the voltages with Artificial Neural Networks. Those approximators provide the advantage to be adapted and optimized to fit new data. If those new data are sampled in the AG-500 measurement field, they can carry information about the perturbed magnetic field and allow distortion correction. They are different potential solutions to use neural networks along with the AG-500. Two alternatives were tested and evaluated in this project:

- Neural Networks interpolating the magnetic field vector.
- Neural Networks interpolating the measured voltages induced between the 2 ends of the sensors by each of the 6 transmitters.

The optimization of the magnetic field model also requires some newly measured data. These data should provide positions and orientations of the sensor coils that are closer to the true ones. This step is also quite challenging. The sensors are tracked in the AG-500 using optimization algorithms that are aimed at minimizing the error between the measured voltages and the predicted ones using the magnetic field model. Therefore, this tracking process is based on the currently used magnetic field model which we want to adapt to improve the accuracy. In order to escape from this vicious circle, we introduced some constraints between the coils which could be utilized as confident knowledge about their

relative positions and orientations. The objective of this solution is to prevent the interpolated observation model, i.e. the relationship between the positions and the orientations of the coils, from degenerating to nonsense when it is optimized with those newly measured data. However, one must find a way to discover the relative positions and orientations of the supposedly fixed coils. In fact, when the coils are fixed on somebody's head at some places where they are supposed to stay fixed relative to each other (forehead, nose, behind the ears...), there is no easy method to accurately measure those relative positions and orientations. In this project, some potential solutions to this problem were evaluated.

6.2 Results

6.2.1 Interpolated observation model

The observation model that links positions and orientations of the coils to the measured voltages was one of the main points of interest in this project, and probably the most time-consuming part. In fact, while artificial neural networks are supposed to be *universal approximators*, this is conditioned by a sufficient amount of hidden units and an appropriate type of activation functions. In this project, different types of networks were trained on one of the two training data sets created from the dipole model and corresponding to the objective of the network. We first assessed the performances on separate validation data sets, and then we used those ANNs to track 4 coils that were fixed relative to each other on a solid block. Then, we observed the tracked distance between those coils. Accurate networks should calculate trajectories of these coils where the distances between two of them are constant.

First, we focused on the problem of interpolating the voltages as a function of the 5 variables describing the state of the coils. Several types of networks were trained on the data set such as single and dual hidden-layered MLP networks, Gaussian radial basis function networks and reverse Hardy's Multi-Quadrics radial basis function networks. Those trainable observation models did not provide satisfactory results. For the best networks, the RMS error on the validation set presented an average difference in the order of 10^{-4} V which could seem satisfactory. However, when we evaluated the performances of these networks using the woodblock with the 4 coils, those proved to be quite bad. The distances between those coils differed by up to 5 mm from the intended fixed distances when the block was relatively steady in the field.

Secondly we dealt with the problem of interpolating the magnetic field vector. The experiments showed that this was possible to model the magnetic field vector with a high precision, which led to the same tracking accuracy as with the dipole model. A Radial Basis Function neural network with 350 hidden units and using the Reverse Hardy's Multi-Quadrics provided the same tracked trajectories of the coils as when this was computed with the *calcamps* function from the TAPADM toolbox (which is based on the dipole model). A Multi-Layered Perceptron with 2 hidden layers of 30 neurons for each layer also performed satisfactorily on the validation set and with the distance evaluation with the woodblock. Gaussian Radial Basis Function networks with 500 hidden units gave satisfactory results with the test of the 4 coils on the woodblock, while the performance on the validation set was much more limited than with the two other types of networks. *Therefore, we conclude that a trainable model for the magnetic field can be obtained.*

6.2.2 Creating a new training data set from measured data

Creating a trainable model of the relationship between the positions and the orientations of the coils and the voltages allows adapting this model to newly measured data in order to mitigate any magnetic field distortions created by perturbations of the environment. We could observe that the dipole model originally used with the AG-500 presented some inaccuracies. Tracking the coils on the solid block with the *calcamps* function that is based on this model provided some random trajectory for the coil n°2, when it was oriented vertically. Therefore, the dipole model should be changed and one way of doing that is to adapt the trainable networks to some measured data which carry the information about the actual magnetic field. However, in order to achieve this training, some confident measured data is required.

In this project, we proposed a solution to get some confident data from the actual magnetic field. We implemented a constrained tracking of 4 coils that were fixed on a solid block. Their relative positions and orientations were known approximately according to the intended ones. Using those constraints between the coils, the trajectory and the orientation of the woodblock, where the 4 coils were fixed on, were tracked using an Unscented Kalman filtering algorithm. Then, given the movement of the block and knowing the position and the orientation of each coil on it, the overall trajectory of each of the 4 coils can be computed. These new trajectories are known to be closer to the true ones, given the knowledge that the coils are fixed relative to each other. These new trajectories along with the corresponding measured voltages are used to create a new training data set. However, as mentioned above, the coil n°2 on the rigid body was inaccurately tracked at some points when we ran the

unconstrained tracking algorithm. Therefore, we compared two versions of the constrained tracking, one using only the 3 coils that did not present these irregularities, and one using the whole set of coils. While the coil n° 2 presented mistaken tracked movements, we observed that the rigid body was tracked more accurately using the 4 coils than only 3. Running the Unscented Kalman filtering algorithm with more constraints provided higher accuracy in tracking the orientation of the block than using fewer constraints and only presumably correctly tracked coils. Therefore, we retained the solution that uses the whole set of coils to track the rigid body.

However, we used the intended positions and orientations of the coils and not the actual precise ones. While the coils were intended to be fixed according to the documentation, their actual positions and orientations might slightly differ from those ones. In this project, we tried to make up for those slight inaccuracies and to discover the actual positions and orientations of the coils on the rigid body. In the constrained tracking, this local arrangement of the coils is used as parameters. A Joint Unscented Kalman filtering algorithm was implemented to optimize jointly the trajectory of the block and the local positions and orientations of the coils on the rigid body. Three different methods were tested. The arrangement of the coils on the block was parameterized in three different ways. All those three methods did not provide satisfactory results and the optimization of the parameters for each of those 3 methods degenerated to nonsense. This suggests that investigating the relative arrangements of coils fixed on a rigid body is a challenging problem. We can venture the hypothesis that discovering the local positions and orientations of coils on a rigid body requires having more constraints on the state of this block, i.e. more coils fixed on it.

However, this experiment with the 4 coils fixed on the block provided knowledge with regard to the coil n° 2. In fact, even if the exact arrangement of the coils on the body could not be discovered, the trajectory and orientation of the block could be accurately tracked using the data from the 4 coils. The movements of the coils 1, 3 and 4 in the global coordinate system were tracked independently with the Unscented Kalman Filter, and those independently tracked trajectories were observed in the local frame of the woodblock. Given that the coils remained almost steady at the same position in the local frame, we could validate the tracked trajectory an orientation of the woodblock, and then infer accurately the actual trajectory of the coil 2.

6.3 Further Works

The overall objective of the project is to find a solution to the observed inaccuracy of the dipole model. In (Zierdt A. , EMA and the crux of calibration, August 2007), A. Zierdt stated that there is probably a "remaining calibration problem" which appears when the sensor orientation becomes parallel to the z-axis. This problem could be observed in this project with the coil n° 2 fixed on the rigid body. Starting from this observation, we proposed to build a trainable model of the magnetic field that could be further optimized with confident measured data. Given that we could obtain a correct interpolation of the magnetic field vector, we continued with the problem of acquiring new confident data. Satisfactory results could be obtained from coils fixed at known distances with known orientations relative to each other. We could not find an easy solution to discover the actual arrangements of the coils on the rigid body that could slightly differ from the intended ones. Therefore, the next steps in this project are the following ones:

- First, to pursue the project further, one would have to find a solution to discover from measured data the local arrangement of coils fixed on a rigid body. A solution to this problem could prove highly useful. In fact, to provide this overall new "calibration" procedure with significant benefits, it would be valuable to acquire these limited data of constrained movements of several coils at the same time as the normal experiments (speech utterances) are done. Gluing some coils behind the ears, on the nose and on the upper part of the jaw (already glued for head correction) and recording the voltage with those ones would provide these data. However, there is no easy way to measure the relative positions and orientations of coils fixed on somebody's head. Having a method to discover the distances and relative orientations between those coils could provide a solution and allow recording the data from the constrained movements at the same time as the normal data. Some new measured data has been acquired by Korin Richmond and Christian Geng from *The Centre for Speech Technology Research of the University of Edinburgh*. They stuck 12 coils on a rigid body at unknown relative distances and orientations and acquired the voltages from long slow movements of the rigid body. These data could be used to investigate a potential solution to the problem of discovering the positions and the orientations of each coil relative to the rigid body.

- Secondly, the trainable model of the magnetic field could be further optimized using those new data obtained from coils fixed with the same distance and orientation relative to each other. There are some potential solutions that can be tried, such as training the network using the new data set, or adapting an Expectation-Maximization algorithm to the problem (see (Haykin, 2001, pp. 175-220)).

Ultimately, if the whole project works and the method is useful, the whole set of methods described above could be combined to implement a solution to calibrate the magnetic field model and to improve the accuracy of the AG-500.

Appendix

Reverse Hardy's Multi-Quadrics

The following code is the core of the implementation of the Reverse Hardy's Multi-Quadrics radial basis networks in Matlab®. It works with other scripts and the Netlab toolbox.

```
function g = rbfbkp(net, x, z, n2, deltas)
% This part of the code was added to the rbfbkp script from the Netlab
% toolbox. This is the core of the implementation of this type of RBF
% network. The rest of the code from this toolbox was slightly modified.

case 'multiquadrics' % Inverse Multiquadrics activation function
   z_cube=z.^3;
   delhid = (delhid.*z_cube);
   % A loop seems essential, so do it with the shortest index vector
   if (net.nin > net.nhidden)
      for i = 1:net.nin
         gc(:,i) = (sum(((x(:,i)*ones(1, net.nhidden)) - ...
            (ones(ndata, 1)*(net.c(:,i)'))).*delhid, 1))';
      end
   else
      for i = 1:net.nhidden
         gc(i,:) = sum((x - (t1*(net.c(i,:)))).*(delhid(:,i)*t2), 1);
      end
   end

   gwi=zeros(1,length(net.wi));
   for i=1:net.nhidden
         gwi(1,i) = sum(-(ones(ndata, 1)*net.wi(i)).*delhid(:,i), 1);
   end
otherwise
   error('Unknown activation function in rbfgrad')
end

g = [gc(:)', gwi, gw2(:)', gb2];
```

Dual Hidden-Layered MLP

The following code is the core of the implementation of the dual hidden-layered MLP networks in Matlab®. It works with other scripts and the Netlab toolbox.

```
function net = mlpdual(nin, nhidden1,nhidden2, nout, outfunc, prior, beta)
% This part of the code was added to the the Netlab toolbox, and was
% written from the mlp script of this toolbox. This creates a dual
% hidden-layered MLP network network. It works with other scripts that
% were implemented from the code of the Netlab toolbox.

net.type = 'mlpdual';
net.nin = nin;
```

```
net.nhidden = [nhidden1 nhidden2];
net.nout = nout;
net.nwts = (nin + 1)*nhidden1 + (nhidden1 + 1)*nhidden2 + (nhidden2 + 1)*nout;

outfns = {'linear', 'logistic', 'softmax'};

if sum(strcmp(outfunc, outfns)) == 0
  error('Undefined output function. Exiting.');
else
  net.outfn = outfunc;
end

if nargin > 5
  if isstruct(prior)
    net.alpha = prior.alpha;
    net.index = prior.index;
  elseif size(prior) == [1 1]
    net.alpha = prior;
  else
    error('prior must be a scalar or a structure');
  end
end

net.w1 = randn(nin, nhidden1)/sqrt(nin + 1);
net.b1 = randn(1, nhidden1)/sqrt(nin + 1);
net.w2 = randn(nhidden1, nhidden2)/sqrt(nhidden1 + 1);
net.b2 = randn(1, nhidden2)/sqrt(nhidden1 + 1);
net.w3 = randn(nhidden2, nout)/sqrt(nhidden2 + 1);
net.b3 = randn(1, nout)/sqrt(nhidden2 + 1);

if nargin == 7
  net.beta = beta;
end
```

```
function g = mlpdualbkp(net, x, z1, z2, deltas)
% This script implements the backpropagation algorithm to compute the
% gradient of the network. I was implemented from the Netlab toolbox.

% Evaluate third-layer gradients.
gw3 = z2'*deltas;
gb3 = sum(deltas, 1);

% Now do the backpropagation.
delhid2 = deltas*net.w3';
delhid2 = delhid2.*(1.0 - z2.*z2); %delhid2 is an (ndata * nhidden2) matrix

% Evaluate second-layer gradients.
gw2 = z1'*delhid2;
gb2 = sum(delhid2, 1);

% Now do the backpropagation.
delhid1 = delhid2*net.w2';
delhid1 = delhid1.*(1.0 - z1.*z1); %delhid1 is an (ndata * nhidden1) matrix

% Finally, evaluate the first-layer gradients.
gw1 = x'*delhid1;
gb1 = sum(delhid1, 1);

g = [gw1(:)', gb1, gw2(:)', gb2, gw3(:)', gb3];
```

The whole code has been implemented from the Netlab toolbox and is available on demand. *(s0898667@sms.ed.ac.uk)*

References

- Bishop, C. M. (2007). *Pattern recognition and Machine Learning.* Springer.
- Carstens, B. *Unbenanntes Dokument*. Retrieved from www.articulograph.de
- Cybenko, G. (1989). Approximation by Superpositions of Sigmoidal Function. *Mathematics of Control, Signal, and Systems* , 303-314.
- Franke, R. (1982). Scattered Data Interpolation: Test of Some Methods. *Mathematics of Computation , 38* (157), pp. 181-200.
- Geng, C., Richmond, K., Renals, S., & Turk, A. (2009). Robust Estimation of Sensor Coil Position and Orientation for Electromagnetic Articulography using an Unscented Kalman Smoother.
- Gorinevsky, D., & Connolly, T. H. (1994). Comparison of Some Neural Network and Scattered Data Approximations: The inverse Manipulator Kinematics Example. *6* (3), 521-542.
- Haykin, S. (2001). *Kalman Filtering and Neural Networks.* John Wiley &Sons, Inc.
- Julier, S. J., & Uhlmann, J. K. (1997). A new extension of the Kalman filter to nonlinear systems. (pp. 182-193). Proceedings of AeroSense: The 11th International Symposium on Aerospace/Defense Sensing.
- Kaburagi, T., Wakamiya, K., & Honda, M. (2005). Three-dimensional electromagnetic articulography: a measurement principle. *Journal of the Acoustical Society of America , 118* (1), 428-443.
- Kelley, C. T. (1999). *Iterative Methods for Optimization.* SIAM Frontiers in Applied Mathematics.
- Lazzaro, D., & Montefusco, L. B. (2002). Radial Basis functions for the multivariate interpolation of large scattered data sets. *140*.
- Møller, M. F. (1993). A scaled conjugate gradient algorithm for fast supervised learning. *6* (4), 525-533.
- Nabney, I. *Netlab neural network software*. (Aston University) Retrieved from www.ncrg.aston.ac.uk/netlab/index.php
- Park, J., & Sandberg, I. W. (1993). Approximation and Radial-Basis-Function Networks. *Neural computation* (5), 305-316.

- Park, J., & Sandberg, I. W. (1991). *Universal Approximation Using Radial-Basis-Function Networks.* Austin, Texas: Massachussetts Institute of Technology.
- Simon, D. J. (2006). *Optimal State Estimation.* John Wiley & Sons, Inc.
- Van der Merwe, R., & Wan, E. A. (2006). *ReBEL*. Retrieved from http://choosh.csee.ogi.edu/rebel/
- Van der Merwe, R., & Wan, E. A. (2001). The square-root unscented Kalman Filter for state and parameter-estimation. *6*, pp. 3461-3464. IEEE.
- Wan, E. A., & Van der Marwe, R. (2000). The Unscented Kalman Filter for Nonlinear Estimation. 153-158.
- Yanusova, Y., Green, J. R., & Mefferd, A. (2009). Accuracy Assessment for AG500, Electromagnetic Articulography. *Journal of Speech, Language, and Hearing Research , 52*, 547–555.
- Zachmann, G. (1997). Distortion Correction of Magnetic Fields for Position Tracking. *Proc. Computer Graphics International* (pp. 213-220). Society Press.
- Zierdt, A. (August 2007). EMA and the crux of calibration. *Institute of Phonetics and Speech Processing* .
- Zierdt, A. *The 3D-EMA Page*. Retrieved from www.phonetik.uni-muenchen.de/~andi/EMAPage/
- Zierdt, A., Hoole, P., & Tillman, H. G. (1999). Development of a system for three-dimensional fleshpoint measurement of speech movements. *Proc. ICPhS.* San Francisco.
- Zierdt, A., Kaburagi, T., Hoole, P., Honda, M., & Tillman, H.-G. (2000). Extracting tongues from moving heads. (pp. 313-316). Germany: 5th Speech Production Seminar.